Available online at www.sciencedirect.com
SCIENCE DIRECT®
PERGAMON
Applied Geochemistry 19 (2004) 29–53
Applied Geochemistry
www.elsevier.com/locate/apgeochem

Modeling sorption of divalent metal cations on hydrous manganese oxide using the diffuse double layer model

Jennifer W. Tonkin[a,*], Laurie S. Balistrieri[b,c], James W. Murray[c]

[a]*Department of Chemistry, University of Washington, Seattle, 98195-1700, Washington, USA*
[b]*U.S. Geological Survey, School of Oceanography, University of Washington, Seattle, 98195-7940, Washington, USA*
[c]*School of Oceanography, University of Washington, Seattle, 98195-7940, Washington, USA*

Received 7 March 2002; accepted 16 April 2003
Editorial handing by M. Kersten

Abstract

Manganese oxides are important scavengers of trace metals and other contaminants in the environment. The inclusion of Mn oxides in predictive models, however, has been difficult due to the lack of a comprehensive set of sorption reactions consistent with a given surface complexation model (SCM), and the discrepancies between published sorption data and predictions using the available models. The authors have compiled a set of surface complexation reactions for synthetic hydrous Mn oxide (HMO) using a two surface site model and the diffuse double layer SCM which complements databases developed for hydrous Fe (III) oxide, goethite and crystalline Al oxide. This compilation encompasses a range of data observed in the literature for the complex HMO surface and provides an error envelope for predictions not well defined by fitting parameters for single or limited data sets. Data describing surface characteristics and cation sorption were compiled from the literature for the synthetic HMO phases birnessite, vernadite and δ-MnO_2. A specific surface area of 746 m^2g^{-1} and a surface site density of 2.1 mmol g^{-1} were determined from crystallographic data and considered fixed parameters in the model. Potentiometric titration data sets were adjusted to a pH_{IEP} value of 2.2. Two site types (≡XOH and ≡YOH) were used. The fraction of total sites attributed to ≡XOH (α) and pK_{a2} were optimized for each of 7 published potentiometric titration data sets using the computer program FITEQL3.2. pK_{a2} values of 2.35±0.077 (≡XOH) and 6.06±0.040 (≡YOH) were determined at the 95% confidence level. The calculated average α value was 0.64, with high and low values ranging from 1.0 to 0.24, respectively. pK_{a2} and α values and published cation sorption data were used subsequently to determine equilibrium surface complexation constants for Ba^{2+}, Ca^{2+}, Cd^{2+}, Co^{2+}, Cu^{2+}, Mg^{2+}, Mn^{2+}, Ni^{2+}, Pb^{2+}, Sr^{2+} and Zn^{2+}. In addition, average model parameters were used to predict additional sorption data for which complementary titration data were not available. The two-site model accounts for variability in the titration data and most metal sorption data are fit well using the pK_{a2} and α values reported above. A linear free energy relationship (LFER) appears to exist for some of the metals; however, redox and cation exchange reactions may limit the prediction of surface complexation constants for additional metals using the LFER.

1. Introduction

Numerous field studies have shown the importance of sorption processes in pristine natural waters, as well as areas affected by acid mine drainage and other industrial activities (Shiller and Boyle, 1985; Honeyman and Santschi, 1988; Fuller and Davis, 1989). Hydrous Mn oxides (HMO), in particular, are important scavengers of trace metals and other contaminants in the environment because of their ubiquitous presence in clays, soils and sediments, their high surface area, and strong affinity for many elements (Jenne, 1968). Sorption is affected by both electrostatic and chemical forces (Sposito, 1983). Manganese oxides can exhibit a low pH point of

* Corresponding author. Fax: +1-206-685-3357.
E-mail address: jtonkin@u.washington.edu (J.W. Tonkin).

0883-2927/03/$ - see front matter
doi:10.1016/S0883-2927(03)00115-X

zero charge (pH_{PZC}) and can develop a large negative surface charge over the pH range of interest in most natural waters (McKenzie, 1981). In addition, the coordination chemistry of metal ions with hydroxyl groups on the HMO surface plays a significant role in sorption (Stumm et al., 1970). The surface properties of Mn oxides have been investigated in both laboratory (Murray, 1974; McKenzie, 1980, 1981; Catts, 1982) and natural (Fuller and Davis, 1989; Tessier et al., 1996; Davis et al., 1998) environments. Recent work (Manceau et al., 1992a; Drits et al., 1997; Silvester et al., 1997; Lanson et al., 2000) has elucidated the diffraction features, crystal structure, and physico-chemical properties of the different birnessite species, making data available for calculating model parameters. Studies of synthetic and natural hydrous Mn oxides, providing details of surface properties and solute sorption, are fundamental to the inclusion of HMO as a sorbing phase in predictive models.

Empirical methods, including partition coefficients, isotherm equations and conditional binding constants, have been employed to describe sorption data (Davis and Kent, 1990). These approaches, however, may not be valid with varying solution chemistry. Surface complexation models (SCMs), which extend the ion-association model of aqueous chemistry to include interactions with solid phases, can be coupled with equilibrium speciation models such as MINTEQA2 (Allison et al., 1991) to describe metal partitioning over a wide range of environmental conditions. The surface complexation approach is, however, complicated by the existence of a variety of competing models. Each SCM has its own physical description of the solid–solution interface and set of thermodynamic data and model parameters, and many provide satisfactory fits to experimental data (Westall and Hohl, 1980; Turner and Sassman, 1996; Venema et al., 1996). Partially as a result of this model flexibility, ion sorption data on Mn oxides have been fit using a number of different SCMs: the triple-layer SCM was used to evaluate and predict surface complexation constants for HMO (Smith and Jenne, 1991), a variation on the constant capacitance model (Schindler and Stumm, 1987) was included in SCAMP (Surface Chemistry Assemblage Model for Particles) to determine model parameters for sorption on Mn oxides (Lofts and Tipping, 1998), crystallographic data were used as the basis for a new surface complexation model formulation (Appelo and Postma, 1999), and a collection of diffuse double layer constants for δ-Mn oxide based upon potentiometric titration data for a single HMO surface have been published (Pretorius and Linder, 2001). Additional SCMS, including the Constant Capacitance (CCM), Basic Stern (BSM), and non-electrostatic (NEM) models have compared favorably with other SCMs in their ability to model proton and cation sorption on additional natural and synthetic mineral surfaces (Davis et al., 1998; Wen et al., 1998; Christl and Kretzschmar, 1999). Whereas the aforementioned investigations provide sets of internally consistent surface complexation constants for HMO and, in some cases, support of the use of a particular SCM, application to systems with multiple sorbing phases remains limited without consistency among the databases for the surfaces considered.

Combining surface parameters for multiple sorbing phases into a complex environmental model requires that experimental data be interpreted consistently with a given SCM, thus making it possible to perform predictive modeling for natural systems of complex and varying composition. Whereas other SCMs have been shown to simulate sorption data well, complementarity of surface complexation constants determined for HMO with those for other important scavenging phases was the primary motivation for this work. Guidelines for a consistent method of compiling and describing experimental sorption data were set forth in a collection of surface complexation constants for hydrous Fe (III) oxide (HFO) (Dzombak and Morel, 1990). Numerous HFO data sets were compiled from the literature and fit using the diffuse double layer SCM, providing for this model an internally consistent database of surface complexation constants. Following these guidelines, databases for goethite (Mathur, 1995) and crystalline Al_2O_3 (Paulson, 1996) were developed, making available a collective set of surface parameters for multiple mineral surfaces. This modeling approach was followed closely and evaluated here for HMO surface and sorption data, with modifications to the criteria for data exclusion, the acid–base model, and the aqueous speciation scheme for model predictions described in further detail below. The result is a complementary set of internally consistent surface complexation constants for sorption of divalent metal cations on HMO for the diffuse double layer SCM.

2. Modeling methods

2.1. Model description

The diffuse double layer SCM, which describes the sorption of solutes at oxide surfaces, is the central component of the generalized two-layer model used to compile a database of surface reactions for hydrous Fe (III) oxide (HFO) (Dzombak and Morel, 1990). This SCM was chosen for this work because of its relative simplicity, its success in describing sorption data for HFO, and its use in the development of complementary databases for goethite and crystalline Al_2O_3. Surface equilibrium reactions are written as a combination of a chemical free energy term, which represents sorption reactions at specific hydroxyl sites on the oxide surface,

and a coulombic term, representative of the electrochemical work of sorption. The coulombic term is calculated from the Gouy–Chapman theory of the electrical double layer and included in the apparent equilibrium constants generated by the model. Both surface property and ion sorption data are necessary components for determining equilibrium constants using the surface complexation model. Specifically, specific surface area (SSA), surface site density, and concentration of a non-specifically adsorbing electrolyte solution are required parameters for the diffuse double layer SCM. The mass of the sorbing phase is desirable; however, molar concentrations can be converted for model input using a formula weight from the literature.

2.2. Data sources

Data for HMO were obtained from an extensive search of the literature. In the cases where data were not tabulated, data were digitized from published graphs. Selected HMO potentiometric titration and cation sorption data sets are shown in Tables 1 and 2, respectively. The following identifiers were used for data sets based upon the system of Dzombak and Morel (1990): 3, HMO solid phase; T, titration data; E, sorption edge; and P, predicted data. The general framework for data selection was based upon methods outlined for HFO (Dzombak and Morel, 1990). Data sets were considered in the cases where HMO solids were similar to naturally occurring Mn oxide minerals with layer structures, and where ionic strength and solid concentration data were available. A suspension density of 1 g l^{-1} for interpretation of charge data and a molecular weight of 119 g mol^{-1} (Giovanoli et al., 1970) were assumed for HMO where necessary. Equilibration times varied; therefore, each study was screened for evidence that equilibrium had been reached with respect to solute uptake. Exclusion of CO_2 in sorption experiments was not considered a criterion for data selection. About half of the data selected was collected under atmospheric conditions and the other half collected under an inert N_2 atmosphere. Due to the lack of carbonate surface complexation constants for HMO, specific sorption of carbonate species was not considered. Variability in the data thus reflects, in part, the presence or absence of CO_2 for the conditions studied.

Determining model parameters by a systematic and reproducible procedure is desirable, (e.g. Dzombak and Morel, 1990). This is difficult for HMO, however, because of the variety and complexity of its several natural and synthetic forms and the relative paucity of surface and sorption data available in the literature. Synthetically prepared oxides are generally used to avoid the complexity of naturally formed particles. Synthetic birnessites, which contain mixed-valency Mn and are generally amorphous in nature, have been commonly used as laboratory proxies for natural HMO. Surface data for several Mn oxides are shown in Table 3. The variability in surface properties is evident even among these synthetic varieties. Required model parameters are

Table 1
HMO Potentiometric Titration Data

ID	Source	Medium	Reported pH_{PZC}
3T1	Murray (1974)	0.0004 M NaCl	⩽2.40, 2.25, 2.15
3T2		0.001 M NaCl	
3T3		0.01 M NaCl	
3T4		0.1 M NaCl	
3T5		0.7 M NaCl	
3T6	McKenzie (1981) solid B44	0.001 M $NaNO_3$	3.0
3T7		0.01 M $NaNO_3$	
3T8		0.1 M $NaNO_3$	
3T9		0.5 M $NaNO_3$	
3T10	Balistrieri and Murray (1982)	0.1 M NaCl	1.5±0.2
3T11		1 M NaCl	
3T12	Catts and Langmuir (1986)	0.001 M $NaNO_3$	2.3±0.2
3T13		0.01 M $NaNO_3$	
3T14		0.1 M $NaNO_3$	
3T15	Fu et al. (1991)	0.001 M $NaNO_3$	–[a]
3T16		0.01 M $NaNO_3$	
3T17		0.1 M $NaNO_3$	
3T18	Ran and Fu (1999)	0.01 M $NaNO_3$	1.48
3T19		0.1 M $NaNO_3$	
3T20		0.5 M $NaNO_3$	
3T21	Pretorius and Linder (2001)	0.1 M KNO_3	–

[a] – indicate no available data.

systematically discussed and evaluated below, with consideration of the unique properties of HMO.

2.3. Model parameters

2.3.1. Specific surface area

A value for specific surface area (SSA) provides a means to normalize solute sorption data to surface area, assuming constant values for SSA and the corresponding number of surface functional groups for the mineral surface considered. The molar concentration of reactive surface sites input to the SCM is calculated from the following values: SSA ($m^2\ g^{-1}$), surface site density ($\mu mol\ m^{-2}$), and measured solid concentration ($g\ L^{-1}$). The SSA value input to the model is taken from individual sorption studies or, as was done here, fixed on the basis of theoretical calculations. Using literature values of unit-cell measurements for Na-birnessite structures (Drits et al., 1997) and MnO_2 formula weight (Giovanoli et al., 1970), the theoretical maximum surface area available, assuming that both sides of the unit cell are available for sorption, is $a \times b = 5.17\ Å \times 2.85\ Å = 44{,}370\ m^2\ mol^{-1}\ MnO_2 \times 2 = 746\ m^2\ g^{-1}$. This calculated value is generally much larger than the values reported for HMO in the literature, which range from 4 (Gray et al., 1978) to 500 $m^2\ g^{-1}$ (Zasoski and Burau, 1988) determined by the methods BET-N_2 and ethylene glycol retention, respectively.

There are several arguments in favor of using a fixed SSA value. First, crystallographic data are available for a direct determination of surface area for synthetic birnessites. Given the ubiquitous presence of birnessite in nature, this determination provides a reasonable proxy value for natural Mn oxides. Second, measured values reported in the literature for Mn oxides are highly variable. This variability may arise from experimental error in the SSA measurement, the effect of ageing or drying on the Mn oxide crystal structure, or inherent differences in the solid surfaces. The BET-N_2 method, which is commonly used to determine SSA for mineral surfaces, may significantly underestimate surface area due to surface decomposition during the drying procedure (Yates, 1975). A value of 600 $m^2\ g^{-1}$ was used for HFO, which is less than a calculated value of 840 $m^2\ g^{-1}$ (Davis, 1977) and more than the 200-300 $m^2\ g^{-1}$ values determined by BET-N_2 and negative sorption methods

Table 2
Cation sorption data sources

Cation	Fit data sets		Predicted data sets	
	Data Identifier	Source	Data Identifier	Source
Ba^{2+}	3EBA1	(Murray, 1975a)	3PBA1	(Gray and Malati, 1979a)
Ca^{2+}	3ECA1	(Murray, 1975a)	3PCA1	(Loganathan and Burau, 1973)
			3PCA2	(Gray and Malati, 1979a)
Cd^{2+}	3ECD1	(Fu et al., 1991)	3PCD1	(Gadde and Laitinen, 1974)
			3PCD2	(Gray and Malati, 1979b)
			3PCD3, 4	(Van der Weijden, 1976)
			3PCD5	(Zasoski and Burau, 1988)
Co^{2+}	3ECO1-10	(Murray, 1975b)	3PCO1	(Loganathan and Burau, 1973)
	3ECO11	(Murray, 1975a)	3PCO2	(Gray and Malati, 1979b)
			3PCO3	(McKenzie, 1980)
Cu^{2+}	3ECU1	(Fu et al., 1991)	3PCU1	(Gray and Malati, 1979b)
	3ECU2-6	(Catts, 1982)	3PCU2	(McKenzie, 1980)
	3ECU7	(Murray, 1975a)	3PCU3	(Stroes-Gascoyne et al., 1987)
Mg^{2+}	3EMG1	(Murray, 1975a)	3PMG1	(Gray and Malati, 1979a)
Mn^{2+}	3EMN1	(Murray, 1975a)	3PMN1	(Gray and Malati, 1979b)
			3PMN2	(McKenzie, 1980)
Ni^{2+}	3ENI1	(Murray, 1975a)	3PNI1	(Gray and Malati, 1979b)
			3PNI2	(McKenzie, 1980)
Pb^{2+}	3EPB1	(Catts, 1982)	3PPB1	(Gadde and Laitinen, 1974)
			3PPB2	(McKenzie, 1980)
			3PPB3	(Nelson et al., 1999)
Sr^{2+}	3ESR1	(Murray, 1975a)	3PSR1	(Gray and Malati, 1979a)
Zn^{2+}	3EZN1	(Catts, 1982)	3PZN1	(Loganathan and Burau, 1973)
	3EZN2	(Catts, 1982)	3PZN2	(Gadde and Laitinen, 1974)
	3EZN3	(Catts, 1982)	3PZN3, 4	(Van der Weijden, 1976)
	3EZN4	(Murray, 1975a)	3PZN5	(Gray and Malati, 1979b)
			3PZN6	(McKenzie, 1980)
			3PZN7, 8	(Zasoski and Burau, 1988)

Table 3
HMO Mineralogy and Surface Data

Source	Mineralogy	O:Mn	pH_{PZC}	SSA ($m^2\ g^{-1}$)	Site density mmol g^{-1}	Site density μmol m^{-2}
Murray (1974)	Birnessite: Low crystallinity; reflections at 1.63, 2.43, 4.04 and 7.4 Å	1.92	2.40 (electrophoresis); 2.25, 2.15 (Na, K adsorption)	263 (BET-N_2)	–[a]	–
McKenzie (1981), B44	Birnessite: X-ray diffraction	–	3.0 (Na exchange capacity at pH 7)	105 (BET-N_2)	2.05 (alkalimetric titration)	22.0
Balistrieri and Murray (1982)	Vernadite or δ-MnO2: Low crystallinity, small diffraction peaks at 1.41 and 2.44 Å	1.96±0.04	1.5±0.2 (potentiometric titration; Na, K, Mg, Ca adsorption)	74 (BET-N_2)	27.2±2.2 (tritium exchange)	367
Catts and Langmuir (1986)	δ-MnO_2: Diffuse peaks at 1.40, 2.35-2.45 Å; a small but distinct peak at 7.0-7.3 Å	–	2.3±0.2 (potentiometric titration; Ca, Na adsorption; electrophoresis)	290 (BET-N_2)	8.6 (tritium exchange)	30
Fu et al. (1991)	δ-MnO_2: Peak at 2.43 Å	1.96		296 (BET-N_2)	4.04 (alkalimetric titration)	13.6
Ran and Fu (1999)	δ-MnO_2: Low crystallinity; diffraction peaks at 1.42, 2.44, and 7.39 Å	1.92±0.09	1.48 (alkalimetric titration, Na adsorption)	93 (BET-N_2)	2.61 (alkalimetric titration)	28.1
Pretorius and Linder (2001)	δ-MnO_2: Peaks at 1.44 and 2.44 Å	–		331 (BET-N_2)	2.9 (alkalimetric titration)	8.8
Davis and Kent (1991)						3.84 (recommended value)
Drits et al. (1997)				746 (theoretical value)	2.1 (theoretical value)	2.8 (theoretical value)

[a] – indicates no available data.

(Dzombak and Morel, 1990). Last, complementary SSA or other surface property data are often unavailable for published HMO sorption data. A theoretical value can be used to model systems where the SSA of the Mn oxide component is unknown. The relatively greater theoretical SSA may be more appropriate for natural systems in which natural Mn oxides, formed by bacteria-catalyzed reactions, may have a much greater SSA than synthetic oxides (Nelson et al., 1999). The authors therefore chose the value of 746 m^2 g^{-1} for all model determinations.

2.3.2. Surface site density and site types

Uncertainty in the surface site density of a given solid phase remains a limitation for surface complexation modeling. For HFO, the total concentration of reactive sites was determined by taking the arithmetic mean of data compiled from the literature (Dzombak and Morel, 1990). Literature values for Mn oxides vary more widely, however, and a mean value may not be appropriate. General use of the value 3.84 μmol m^{-2} as a close approximation of surface site density for all minerals has been recommended (Davis and Kent, 1990). However, crystallographic calculations for bulk mineralogical structure are currently considered most appropriate for determining site density for sorption processes; ^3H exchange calculations, which measure hydroxyl groups that are structurally unavailable for ion sorption, are considered unrealistically high (Goldberg, 1998). Surface site density values are most often normalized by a SSA value and reported per unit area. Measurement of surface site density values per mass of solid phase, however, avoids likely uncertainties in SSA measurements.

X-ray and selected-area electron diffraction (XRD, SAED) methods were used to provide a detailed description of the distribution of layer Mn cations and the structure of interlayer cations in Na-birnessites, with reported formulae varying from $Na_{0.33}Mn^{4+}_{0.67}Mn^{3+}_{0.33}$ to $Na_{0.167}Mn^{4+}_{0.833}Mn^{3+}_{0.167}$ (Drits et al., 1997). Assuming that the Na stoichiometries represent the maximum content of Na atoms per layer octahedron, or mol surface sites mol Mn^{-1}, site densities of 1.40–2.80 mmol sites g^{-1} HMO were calculated using a formula weight of 119 g mol^{-1} (Giovanoli et al., 1970). The average value of 2.10 mmol sites g^{-1} HMO was used for all model simulations. If Mn oxides are well characterized as birnessite or Mn oxides with layer structures, this type of calculation precludes the introduction of errors by secondary measurements of SSA and site density.

For HFO, reactive sites at the oxide surface were divided into two types: Type 2 sites, the total reactive sites available for sorption of protons, cations, and anions as determined from observed sorption maxima; and Type 1 sites, a smaller set of high-affinity cation binding sites, the density of these sites determined from sorption isotherms as the sorption density at which sorption becomes less than proportional to dissolved concentration (Dzombak and Morel, 1990). HFO Type 1 and Type 2 surface site densities were derived from a compilation of measurements available in the literature. Density estimates for high and low affinity surface sites on HMO, however, are not available. The total surface site density value for HMO was calculated from crystallographic data (Drits et al., 1997) and fixed in all subsequent model calculations. For HMO, the fixed total concentration of surface sites (g^{-1}) was divided into fractions of two site types (≡XOH and ≡YOH) which were used to describe sorption reactions on HMO.

2.4. FITEQL modeling

The determination of surface equilibrium constants from experimental data was performed using the computer program FITEQL3.2 (Herbelin and Westall, 1996) and the diffuse double layer SCM. Data were modeled using tabulated solution equilibrium constants and activity coefficients for dissolved ionic species (Dzombak and Morel, 1990). Ionic strength corrections were performed using the Davies equation and parameters $A = 1.17$ $mol^{-1/2}$ $L^{1/2}$ and $b = 0.24$; supplemental activity coefficients for $I > 0.1$ M were found elsewhere (Morel, 1983). pH data were corrected to concentration units for input into FITEQL3.2. Log K values for all dissolved ionic species were corrected to the appropriate ionic strength. Log K values for mass action expressions for the sorption reactions determined within the model framework included the coulombic correction factors. All resulting log K values were therefore corrected to $I = 0$ and reported as intrinsic constants. A curve-by-curve approach was used to capture the variability in sorption onto HMO. A best fit including all data sets was obtained by weighting the parameter estimate from an individual data set on the basis of its standard deviation calculated in FITEQL3.2. The statistical procedure employed was taken from Dzombak and Morel (1990) and is described in detail therein. The equilibrium speciation model MINTEQA2 (Allison et al., 1991) and its thermodynamic database was used to reproduce model fits to the experimental data.

2.4.1. Charge data

Seven potentiometric titration data sets were chosen to determine pK_{a2} values for HMO (Murray, 1974; McKenzie, 1981; Balistrieri and Murray, 1982; Catts and Langmuir, 1986; Fu et al., 1991; Ran and Fu, 1999; Pretorius and Linder, 2001). These data were chosen based upon the similarity of the surface studied to naturally-occurring Mn oxide minerals with layer structures; e.g.; minerals of the poorly crystalline birnessite group ([Na,Ca,Mn(II)]$Mn_7O_{14}{\cdot}2.8H_2O$) or vernadite ($MnO_2{\cdot}nH_2O$), analogous to the synthetic phase δ-MnO_2. Data sets and surface properties are shown in Tables 1 and 3.

Charging curves for several Mn oxides determined at a common ionic strength of 0. 1 M are shown in Fig. 1. The charge data were normalized to grams of Mn oxide and plotted as a function of measured pH. Differences in the oxide surfaces are apparent with respect to both the intersection of the curves with zero charge and the change in charge as a function of pH. A common method for determining the pH_{PZC}, the unique pH value at which the charge due to protons and hydroxide ions bound to the mineral surface is equal to zero, for simple oxides is to calculate net titration curves, or charging curves, at several ionic strengths and determine their intersection. Titration measurements are difficult to make at low pH values, because of the steep nature of the titration curve and the possibility of reduction of H_2O under these solution conditions. For Mn oxides with low pH_{PZC} values, errors in titration measurements are potentially large. Within sets of charging curves collected from the literature for a given HMO surface, charging curves may appear parallel and there are few actual points of intersection. Additionally, visual extrapolation of the charging curves to a common point does not necessarily suggest a pH_{PZC} consistent with the reported value.

Charge data were adjusted where necessary to a common pH_{IEP}, or the pH value at which the surface has no counterion charge, of 2.2. This value agrees with those determined by electrophoretic measurements reported in the literature (Murray, 1974; Catts and Langmuir, 1986). Adjustment of the data to a common pH_{IEP} accounts for possible separation of the pH_{PZC} and pH_{IEP} resulting from sorption of additional cations or anions on the surface. Data sets were adjusted by anchoring at a single point, thus preserving relationships among the titration curves including effects of changing ionic strength. The adjustment procedure is described for data with a reported pH_{PZC} of 1.48 (Ran and Fu, 1999). First, the net titration curve at the highest ionic strength was chosen as, of a family of alkalimetric titration curves, experimental data at the highest ionic strength show the most linear relationship between charge and pH. Second, a line was drawn from the data point (pH = highest measured pH value, corresponding M *TOT*H value) to the artificial point (pH = 1.48, M *TOT*H = 0). The slope of this line and the data point were used to determine the M *TOT*H, or charge correction necessary to adjust the *y*-intercept, or pH_{IEP} value to 2.2. Last, this single correction value was applied to all titration data points. Data sets with reported pH_{PZC} values of 3.0, 1.5 and 2.3 (McKenzie, 1981; Balistrieri and Murray, 1982; Catts and Langmuir, 1986), respectively, were adjusted in a similar manner. No pH_{PZC} value was reported in Fu et al., (1991), but the authors cited the value 2.8 (Morgan and Stumm, 1964). It was assumed that data were adjusted to this value and corrected all titration data points using the method described above. No pH_{PZC} value was reported in Pretorius and Linder (2001); further, the data are reported as mM *TOT*H, making it unclear whether the data were adjusted to zero charge. Where a published correction factor was available (Murray, 1974), this value was used to correct all titration data.

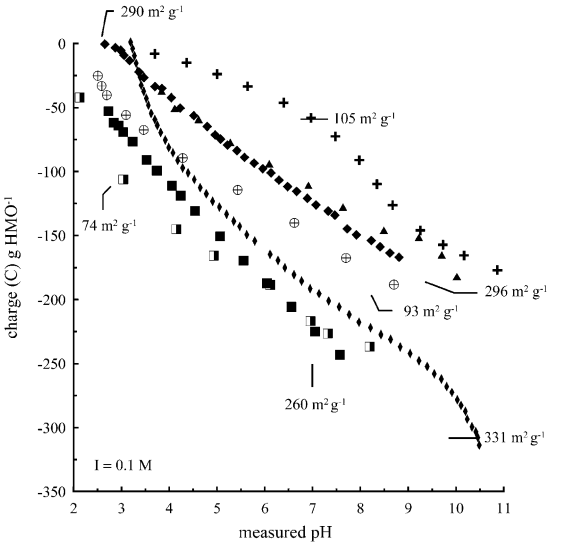

Fig. 1. HMO surface charge (C g^{-1}) as a function of pH at $I = 0.1$ M. Data shown are not adjusted to a common pH_{IEP}; reported pH_{PZC} values for the individual data sets are shown in Table 1. Data sources are as follows: ■ (Murray, 1974), + (McKenzie, 1981) ◨ (Balistrieri and Murray, 1982), ◆ (Catts and Langmuir, 1986), ▲ (Fu et al., 1991), ⊕ (Ran and Fu, 1999), ♦ (Pretorius and Linder, 2001). Specific surface area measurements (m^2 g^{-1}) determined by BET-N_2 are shown for reference.

A two-site model was employed to describe acid-base reactions at the HMO surface, and the following reactions were used in FITEQL3.2:

Acid−base reactions:

$$\equiv XOH = \equiv XO^- + H^+ \quad K_{a2\equiv XOH}$$
$$\equiv YOH = \equiv YO^- + H^+ \quad K_{a2\equiv YOH}$$

The monoprotic surface sites are consistent with the reactive sites defined for HFO (Dzombak and Morel, 1990). The total site concentration was fixed at 2.1 mmol g^{-1} and the concentrations of ≡XOH and ≡YOH for a given HMO solid from a given research group were determined by the parameter α (the fractions ≡XOH and ≡YOH equal to α and 1-α respectively). For most data sets, data points at the lower pH values appeared to have large associated errors and questionable data points at the lowest pH values were removed before fitting the data. $pK_{a2\equiv XOH}$ and $pK_{a2\equiv YOH}$ were considered adjustable parameters, and α was initially adjusted manually until the lowest least-squares error

(WSOS DF^{-1}) value was reached. α was expected to be constant within a research group, and, in most cases, the same α value gave the lowest WSOS DF^{-1} value for a set of titration data. In the cases where α varied slightly, the α value was chosen based upon applicability of the data to a natural system (i.e. the ionic strength at which the titration curves were determined). The single, or optimal, value of α determined for each HMO solid was used as a fixed parameter to determine the optimal $pK_{a2\ \equiv XOH}$ and $pK_{a2\ \equiv YOH}$ and WSOS DF^{-1} values for each titration data set. A best α value was calculated by averaging the α values determined for each research group. Best $pK_{a2\ \equiv XOH}$ and $pK_{a2\ \equiv YOH}$ values were calculated by weighting the parameter estimates from the individual data sets based upon their standard deviation values calculated in FITEQL3.2 and determining the weighted average.

The statistical *F*-test (Hamilton, 1965) is used as a model comparison test to select from two competing models that describe a particular data set, e.g., a one- or two-site model. The *F*-ratio describes the improvement, or decrease, in the weighted sum of squares of errors (WSOS) relative to the loss in degrees of freedom (DF) when going to a higher-constrained model, i.e., one with a greater number of adjustable parameters. The *F*-test was applied and an *F*-ratio calculated from model fits to all titration data sets. The calculated *F*-ratios were compared to tabulated F values at DF_1, the change in degrees of freedom between the two models, DF_2, the total degrees of freedom in the more complicated model, at $\alpha = 0.05$. A 3-site model, with manually optimized α and β values, was also examined. These comparisons were used to choose between one- two- or three-site surface models for each set of titration data. pK_{a1} values were not considered as there were, in most cases, insufficient data below the pH_{PZC} to obtain model convergence; where the model converged, *F*-tests indicated that the addition of the $\equiv YOH_2^+$ species did not significantly improve model fits. The optimal and best model fits were generated using MINTEQA2 and its thermodynamic database and plotted for each titration data set along with all titration data points. In addition, two curves generated using the best $pK_{a2\ \equiv XOH}$ and $pK_{a2\ \equiv YOH}$ values and the high and low α values were plotted for each data set.

2.4.2. Cation data

The following reactions were used in FITEQL3.2 to model cation sorption on the HMO surface:

Cation(Me^{2+})sorption:

$$\equiv XOH + Me^{2+} = \equiv XOMe^{+} + H^{+} \qquad K_{XOMe+}$$

$$\equiv XOH + Me^{2+} + H_2O = \equiv XOMeOH + 2H^{+} \qquad K_{XOMeOH}$$

$$\equiv YOH + Me^{2+} = \equiv YOMe^{+} + H^{+} \qquad K_{YOMe+}$$

$$\equiv YOH + Me^{2+} + H_2O = \equiv YOMeOH + 2H^{+} \qquad K_{YOMeOH}$$

Three research groups provided both titration data and cation sorption data for the same HMO solid (Murray, 1974; Catts, 1982; Catts and Langmuir, 1986; Fu et al., 1991). For these cation sorption data sets, the optimal α value determined for the corresponding titration data sets was fixed and log *K* values for the metal sorption reactions were considered adjustable parameters in the model. Sorption data for Ba^{2+}, Ca^{2+}, Cd^{2+}, Co^{2+}, Cu^{2+}, Mg^{2+}, Mn^{2+}, Ni^{2+}, Pb^{2+}, Sr^{2+}, and Zn^{2+} were fit using FITEQL3.2. Best $pK_{a2\ \equiv XOH}$ and $pK_{a2\ \equiv YOH}$ values were used to fit all cation sorption data. Optimal values of the surface complexation constants log K_{XOMe+}, log K_{XOMeOH}, log K_{YOMe+}, and log K_{YOMeOH} were determined for each metal sorption data set using the optimal α value. Model fits were determined using a sequential determination of sorption constants, with the *F*-test applied after each addition. A surface species was included if it was statistically significant in fitting the data; however, a surface species was rejected if it consistently produced high standard deviations (S.D.). Sorption of both the free metal cation and the first metal hydrolysis product were necessary to obtain the best fit for most data sets. Best estimates of the constants were calculated by weighting the parameter estimates from the individual data sets based upon their standard deviation values calculated in FITEQL3.2. High and

Table 4
Best estimates for HMO acidity constants, $I = 0$

Best α Value	Best Estimate log *K*	Confidence Level (%)	log *K* (+)	log *K* (−)
0.64	log $K_{a2\ (XOH)} = -2.35$	99	−2.241	−2.450
		95	−2.269	−2.422
		90	−2.282	−2.409
		80	−2.297	−2.394
	log $K_{a2\ (YOH)} = -6.06$	99	−6.000	−6.112
		95	−6.017	−6.096
		90	−6.024	−6.089
		80	−6.032	−6.081

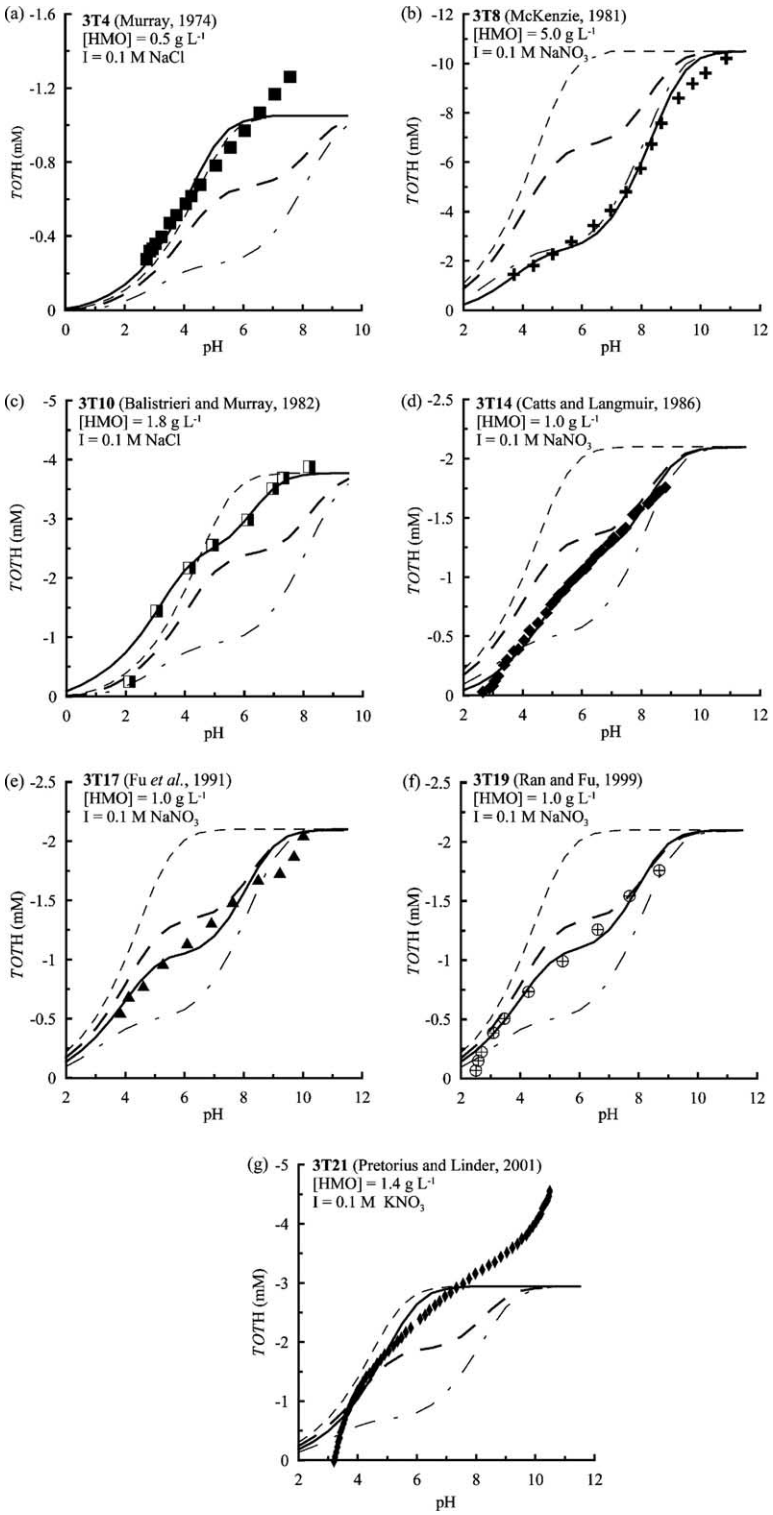

Fig. 2. Model fits to acid–base titration data plotted as net protons released by HMO (*TOT*H) vs. measured pH. Data identifiers and sources are referenced in Table 1. Experimental data are shown by the symbols. Optimal and best model fits to the data are shown by the solid and dashed lines, respectively. Model fits using best pK_{a2} values and high and low α values are shown by the pale small dash and dot dash lines, respectively. Data have been adjusted to a pH_{IEP} of 2.2; unadjusted data are shown in Fig. 1.

low log K values at the 99, 95, 90 and 80% confidence levels were calculated using tabulated values of Student's t. Optimal and best model fit curves were generated using MINTEQA2 and plotted for each cation sorption data set. Two additional curves using the best cation sorption log K values and high and low α values were generated and plotted for each data set. Curves using best log K values and the low, average, or high α values were also generated and compared with cation sorption data sets for which complementary titration data were not available.

3. Results and discussion

3.1. Structure of manganese oxides

Hydrous Mn oxide minerals are assembled from MnO_6 octahedra that can be arranged in a number of different structural arrangements, most of which fall into two major groups: (1) chain, or tunnel structures and (2) layer structures (Post, 1999). Generally, Mn oxides with layer structures consist of stacked sheets of MnO_6 octahedra, with specific differences in the occurrence of layer vacancies and the types of cations that are sandwiched between the layers to balance the negative charge. Chalcophanite ($ZnMn_3O_7{\cdot}3H_2O$) has been often used as a model for layer-type Mn oxide minerals (Giovanoli et al., 1970; Burns and Burns, 1979; Drits et al., 1997) because it has structural characteristics similar to the environmentally ubiquitous birnessite. The chalcophanite structure consists of sheets of edge-sharing $Mn(IV)O_6$ octahedra, with one out of every 7 Mn(IV) cations replaced by a layer vacancy. The resulting negative layer charge is compensated for by two Zn(II) cations in the interlayer region positioned above and below the vacancy. Recent studies (Drits et al., 1997; Silvester et al., 1997; Lanson et al., 2000) have elucidated variations in diffraction features, crystal structure, and physico-chemical properties within the birnessite species, providing details for a closer analog for Mn oxides with layer structures.

Both layer charge and Mn oxidation state contribute to structural heterogeneity in synthetic Mn oxides. Negative structural charge in HMO arises from the formation of site vacancies within the layers, and from the substitution of Mn(III) for Mn(IV) cations in the layer octahedra (Post, 1999). Manganese oxides with a higher Mn oxidation state are likely to possess more site vacancies, as a result of the disproportionation of layer Mn(III) into layer Mn(IV) and solution Mn(II). Polarized EXAFS studies indicated a high proportion of layer Mn(III) and an insignificant number of layer vacancies in synthetic Na birnessite, with the layer charge resulting from the substitution of lower-valent Mn (Silvester et al., 1997). MnO_6 octahedra may be edge- or corner-sharing, with corner-sharing octahedra positioning themselves above vacant layer sites. Birnessite is proposed as an end-member with the highest ratio of structural edge- sharing to corner-sharing octahedra. Synthetic δ-MnO_2, considered representative of natural vernadite, is disordered in its layer stacking and has both edge- and corner-sharing octahedra (Manceau et al., 1992a). Structural differences resulting from layer charge and Mn oxidation state could result in heterogeneity of reactive sites on the HMO surface. Oxygen atoms coordinated to different-valent Mn cations have varying degrees of undersaturation of positive charge. Reactive surface sites at layer vacancies or at layer sites are therefore postulated to sorb cations with varying affinities.

Monoprotic sites were chosen to describe cation sorption at the HMO surface. Structural data suggest that the 3 oxygens at a site vacancy are coordinated with

Table 5
HMO cation surface complexation constants, $I=0$

log K_{MeOH}	Cation (Me^{2+})	Best Estimate log K			
		≡XOMe$^+$	≡XOMeOH	≡YOMe$^+$	≡YOMeOH
0.53	Ba^{2+}	0.45	–[a]	–	–
1.15	Ca^{2+}	−1.5	–	–	–
3.92	Cd^{2+}	−2.4	−8.0	−3.5	−8.5
4.35	Co^{2+}	1.0 (0.1)[b]	−3.9 (0.6)	–	–
6.5	Cu^{2+}	0.85 (0.36)	−2.8 (0.3)	0.86 (4.12)	−5.7 (1.0)
2.56	Mg^{2+}	−2.4	−7.7	–	–
3.41	Mn^{2+}	1.2	−2.7	–	–
4.14	Ni^{2+}	−0.48	−5.0	–	–
6.29	Pb^{2+}	–	−0.86	3.4	−1.6
0.71	Sr^{2+}	−1.6	−6.6	–	–
5.04	Zn^{2+}	−0.010 (0.779)	−4.4 (1.2)	–	−7.6 (4.7)

[a] – lines indicate no estimate of log K from data fits.
[b] Values listed in parentheses are errors at the 95% confidence level.

two Mn (IV) cations, giving each O an excess negative charge of 2/3, whereas each O at a layer Mn(III) site, where the oxygens are coordinated to two Mn(III) and one Mn(IV), has an excess charge of 1/3 (Drits et al., 1997; Appelo and Postma, 1999). An SCM using an HMO surface site formulation of $\equiv SO_3H_2$, consistent with the valency of Mn at the vacant sites, was recently proposed (Appelo and Postma, 1999). This SCM, however, does not account for possible site heterogeneity and, although it takes into account detailed structural information, is inconsistent with the primary objective of complementarity with existing models using the diffuse double layer SCM. In the context of a ≡SOH surface site formulation, it is proposed that the average oxidation state of Mn at a site vacancy is higher than at a layer site, given the excess surface charge for the individual O atoms calculated as above. Transition metals have been shown to sorb at Mn oxide layer vacancies (Manceau et al., 1992a), but a 5-coordinated Mn(III) cation could also bind a metal atom as is proposed for sorption on HFO (Dzombak and Morel, 1990). Reported oxidation states for HMO used in this study vary from 1.96±0.04 (Balistrieri and Murray, 1982) to 1.92 (Murray, 1974; Ran and Fu, 1999). Assuming a higher-oxidized HMO possesses more site vacancies, variations in oxidation state could reflect varying proportions of layer and vacant sites. It is impossible to know the exact structures of the HMO used to determine the HMO

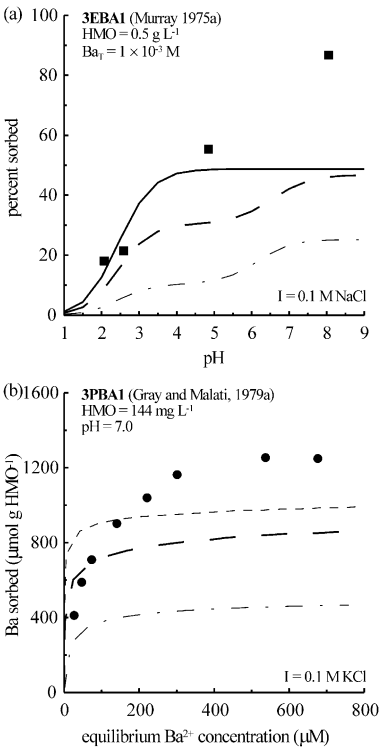

Fig. 3. Model fits and model predictions for cation sorption data for Ba, Ca, Cd, Co, Cu, Mg, Mn, Ni, Pb, Sr, and Zn. Data identifiers and sources are referenced in Table 2. Experimental data are shown by the symbols. Fit data sets are designated by the prefix 3E; predicted data sets by the prefix 3P. Optimal (using parameters for individual data sets) and best (using weighted average parameters) model fits to the data are shown by the solid and dashed lines, respectively. Model fits using best log K values and high and low α values are shown by the pale small dash and dot dash lines, respectively. For predicted data sets, model predictions using best log K values and α values of 0.24, 0.64, and 1.0 are shown by the pale dot dash, dashed, and pale small dash lines, respectively. For all Figs. the error envelope is shown by the curves generated with the high and low α values.

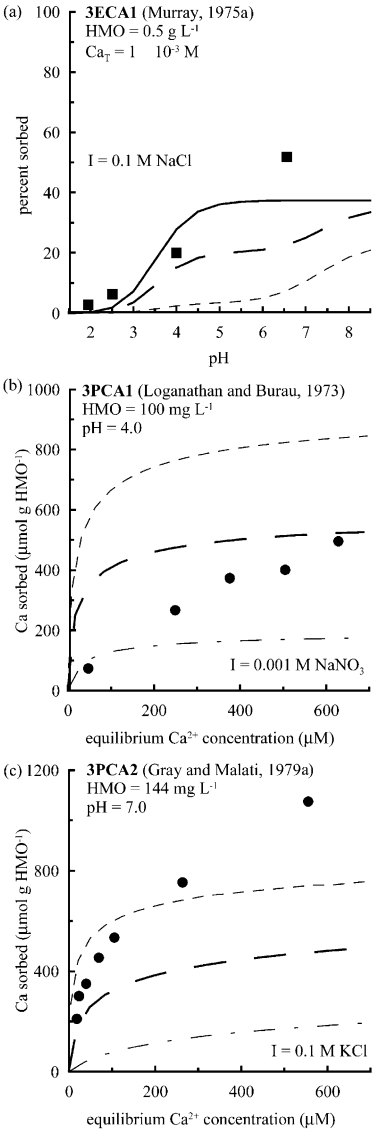

Fig. 4. Please refer to Fig. 3 caption for information.

parameters presented here. However, recognizing differences in geometry and variations in Mn valency at possible binding sites on the HMO surface is important in constructing a generalized multiple-site model.

3.2. Two-site model

A model with a greater number of parameters can always fit experimental data at least as well as that with fewer parameters, given that the simpler of the two models is nested within the other, i.e. one can obtain the simpler model by setting the extra parameters of the more complex model to default values, often zero. The results of the statistical *F*-tests showed that, for 5 of the 7 titration data sets, the two-site model fit the data significantly better than the one-site model. For one data set (Murray, 1974), there was not a consistent result. *F*-ratios determined for titration data at $I = 0.01$ and 0.7 M NaCl suggested that a one-site model was adequate to fit the data; however, *F*-ratios for data at $I = 0.0004$, 0.001 and 0.1 M NaCl suggested that a two-site model gave a significantly better fit. The α value describing the proportions of the different site types was expected to be constant for a given research group. For this data set, however, manual optimization of α to the lowest least-squares error value gave inconsistent results among the individual charging curves. These data were therefore fit with the simpler one-site model. A one-site model was sufficient for one data set (Pretorius and Linder, 2001). A three-site model was also considered. *F*-tests were

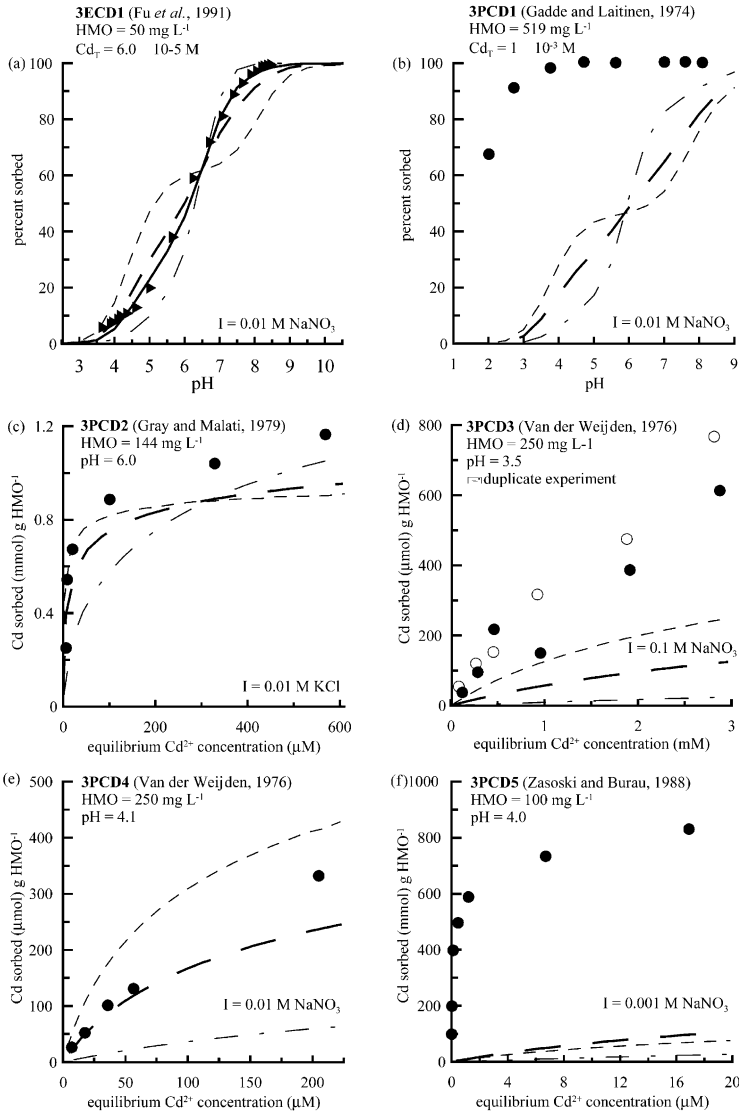

Fig. 5. Please refer to Fig. 3 caption for information.

performed on results from simulations in which the model converged. The statistical tests did not indicate consistent improvements in the model fits to the titration data using the three-site model, therefore the simpler two- or one-site models were used where appropriate.

Pretorius and Linder (2001) considered total surface site densities in addition to log K values as adjustable parameters in a proposed two-site HMO surface model. The authors considered site concentrations and pK_a values as adjustable parameters and selected the best model using the statistical F-test. They determined an optimal total site concentration of 3.0 mmol g^{-1}, which is 1.4×greater than the value used in this work. Interestingly, with the additional parameter adjustments, the

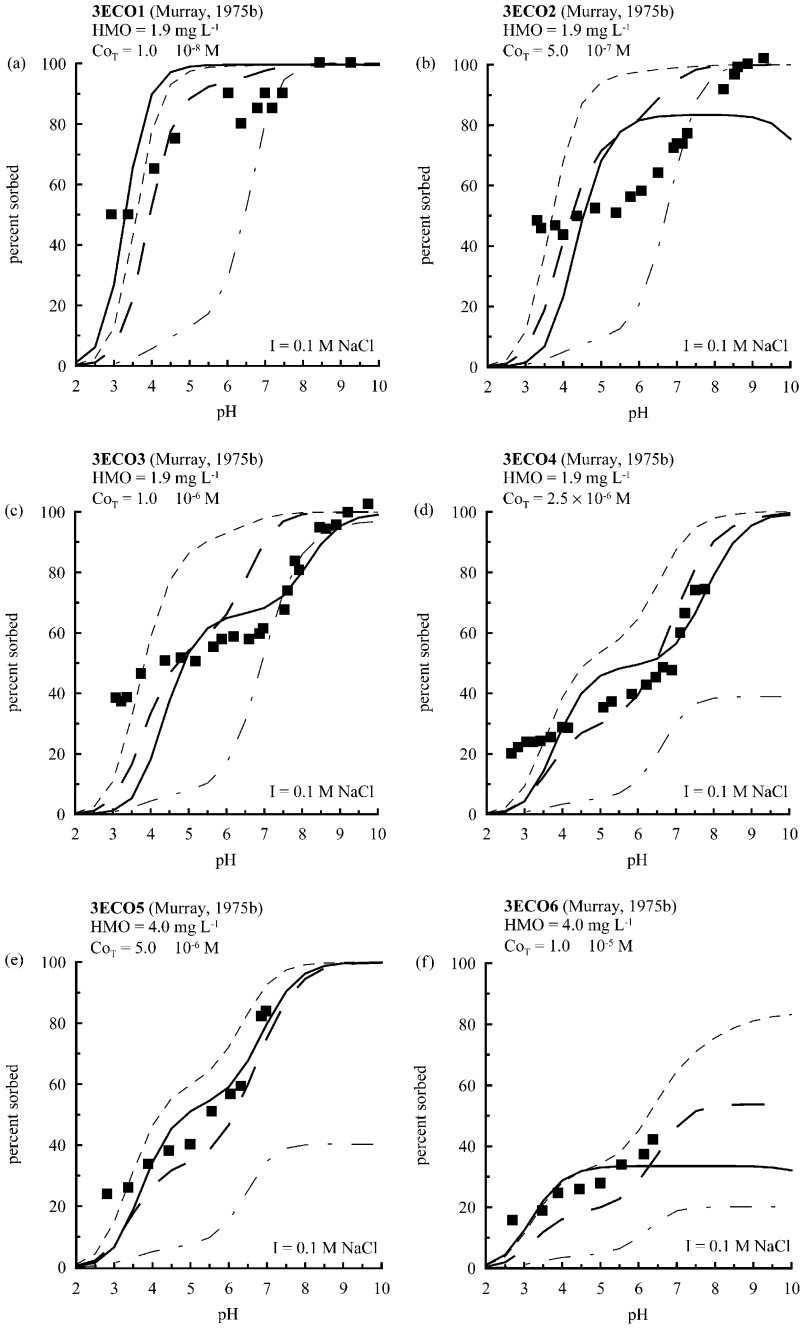

Fig. 6. Please refer to Fig. 3 caption for information.

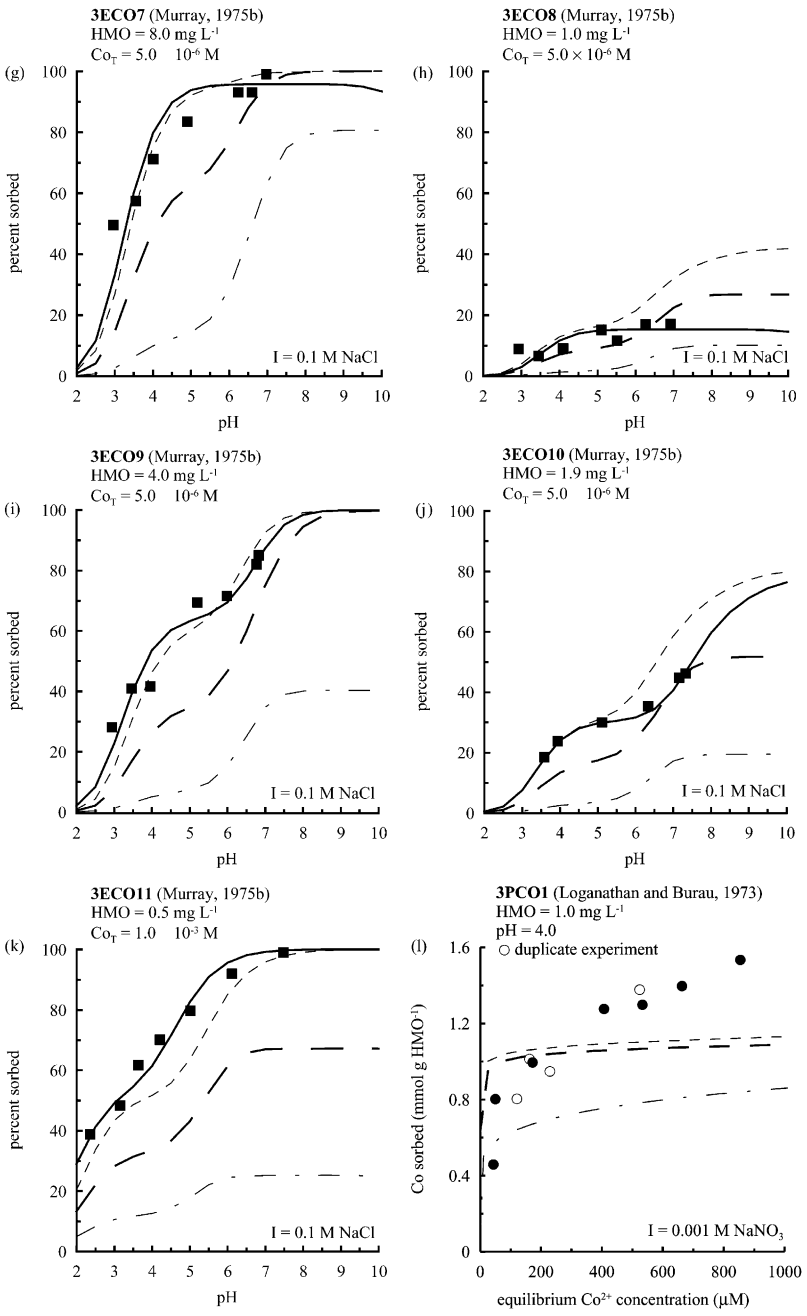

Fig. 6 (*continued*).

authors concluded that the titration data were fit significantly better with the two-site model than with the one-site model. Using the authors fixed total site concentration of 2.1 mmol g^{-1}, however, it was concluded from the *F*-test that a one-site model was sufficient to describe their titration data. It is reasonable to propose a two- or multiple-site model given the available HMO structural information. One should, however, conclude with caution that any n-site model gives a unique description of the HMO surface, as the result is clearly dependent on the choice of total site concentration.

3.3. Surface characteristics and charge data

HMO data sets and the reported physio-chemical properties are shown in Tables 1 and 3. Although these

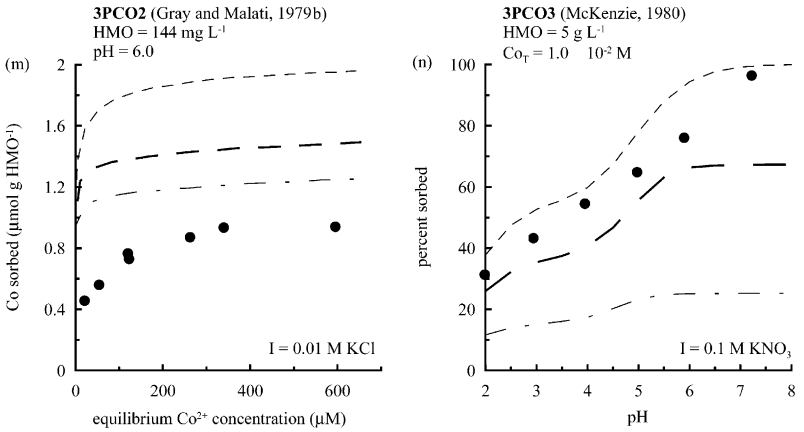

Fig. 6 (*continued*).

data were selected on the basis of similarities to natural-occurring Mn oxide minerals with layer structures, the tabulated data show differences among HMO phases in measured pH_{PZC}, SSA, and surface site density. Variations among the accumulation of charge as a function of pH, illustrated in Fig. 1, suggest that the sorbent composition may be varying among different HMO preparations. Even with adjustment to a common pH_{IEP}, all curves at a given electrolyte concentration were not coincident.

Optimal α values for each research group and optimal log $K_{\equiv XOH}$ and log $K_{\equiv YOH}$ values with corresponding S.D. for each titration data set are shown in Appendix A. α values ranged from a low value of 0.24 (McKenzie, 1981) to a high value of 1.0 (Murray, 1974; Pretorius and Linder, 2001), with an average value of 0.64. Optimal log $K_{\equiv XOH}$ and log $K_{\equiv YOH}$ values corrected to $I=0$ were consistent within most data sets. Agreement among the optimal log $K_{\equiv XOH}$ and log $K_{\equiv YOH}$ values determined for different research groups is a strong point in applying the two-site surface model; this consistency supports the hypothesis that the total surface site concentration of the HMO solids is composed of two end-member site types, with the relative site type concentrations described by the optimal α values. The calculated average, or best α value and best values of log $K_{\equiv XOH}$ and log $K_{\equiv YOH}$ are shown in Table 4. Errors of 0.11 and 0.06 log units at the 99% confidence level are minimal for log $K_{\equiv XOH}$ and log $K_{\equiv YOH}$ values of -2.35 and -6.06, respectively, and lend support to the two-site hypothesis. Given the aforementioned structural information and the context of the authors surface site formulation, a Mn cation at a layer vacancy is considered to have a relatively higher net oxidation state than a layer cation. An O coordinated to a more highly-charged cation is expected to hydrolyze more easily (Hugheey et al., 1993); thus, a lower pK_a value for a site vacancy is expected relative to that for a layer site. The resulting best values of log $K_{\equiv XOH}$ and log $K_{\equiv YOH}$ are consistent with this structural hypothesis. It remains impossible, however, to know the exact structures of the HMO solids studied.

Model fits to adjusted titration data at $I=0.1$ are shown in Fig. 2. The error envelope generated using the best log $K_{\equiv XOH}$ and log $K_{\equiv YOH}$ values and the low and high α values illustrates the variation in HMO surface behavior reflected by the α value, which, for predictive modeling, may be an unknown parameter. In general, model fits using the two-site model and optimal log K values simulate the data well. However, variability among HMO surfaces is apparent in the best model fits. The experimental data shown in Fig. 2(a) (Murray, 1974) and 2(g) (Pretorius and Linder, 2001) were not fit well by the model. The predicted curves flatten out at a *TOT*H value characteristic of the fixed surface site density value. This saturation of sites is not seen in the experimental data, however, suggesting that the surface site density may be higher for these HMO solids than the fixed value chosen here. Pretorius and Linder (2001) obtained a more satisfactory model fit to the data in Fig. 2(g) considering surface site density an adjustable parameter.

3.4. Cation sorption

Ideally, both potentiometric titration data and cation sorption data were available for a single HMO solid. The availability of complementary titration data allowed for the determination of α and pK_a values specific to a given solid preparation. These values were used as model parameters to fit the cation sorption data and determine the best estimates of HMO cation surface complexation constants. Available sources providing both sets of data were limited in number. However, several cation sorption data sets without accompanying titration data were available in the literature. In the

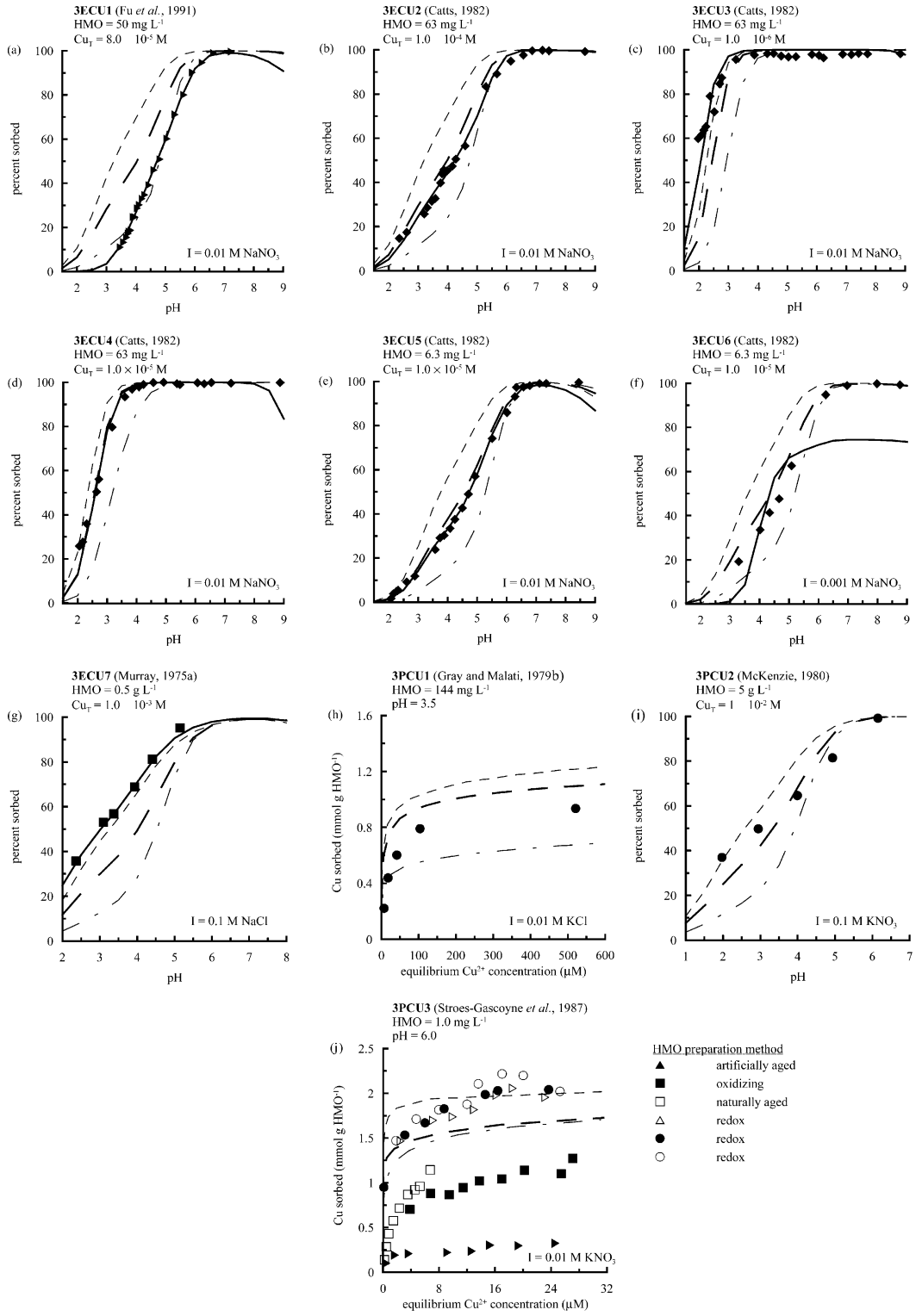

Fig. 7. Please refer to Fig. 3 caption for information.

cases where only cation sorption data were available, the best estimates of HMO constants were used to test the agreement between model predictions and experimental data as a function of α. Both fit and predicted data sets are shown in Table 2. Only a single data set was available for determining best estimates of surface complexation constants for several metals. However, model predictions of additional cation sorption data sets using the best parameters allowed the authors to test both the model's accuracy and its ability to capture differences among HMO solids.

Best estimates of cation surface complexation constants at $I=0$ for Ba^{2+}, Ca^{2+}, Cd^{2+}, Co^{2+}, Cu^{2+}, Mg^{2+}, Mn^{2+}, Ni^{2+}, Pb^{2+}, Sr^{2+}, and Zn^{2+} are shown in Table 5, with errors at the 95% confidence level shown in parentheses. Errors at additional confidence levels are shown in Appendix B. Error values are high in most cases; however, a limited number of data sets for model fitting were available for most metals. In the cases where cation sorption data from a single data source was fit, no error value is shown. A comparison of constants determined for ≡XOH and ≡YOH surface sites for the same metal and surface species shows that sorption is weaker for the ≡YOH site type, consistent with its greater corresponding pK_a value.

Both model fits to cation sorption data sets with complementary titration data and model predictions of additional cation sorption data using the best estimate surface complexation constants are shown for each metal in Figs. 3–13. Model fits to the experimental data are good, with the exception of the alkaline earth cations. Model simulations predict the data well in most cases, with the experimental data falling within the error envelope. Fits and predictions for Cu and Pb illustrate

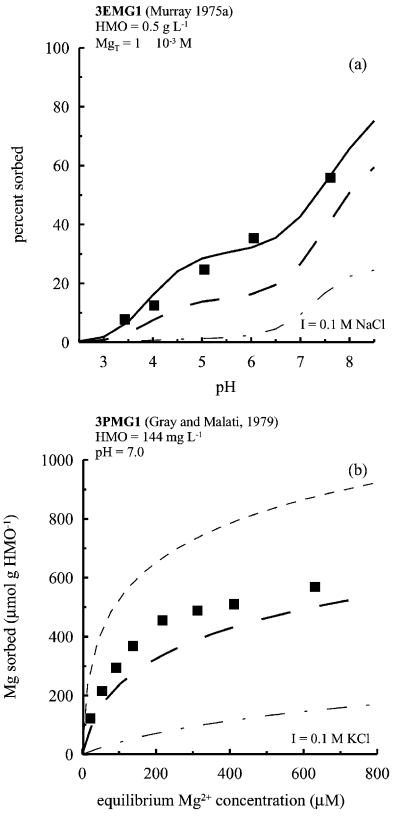

Fig. 8. Please refer to Fig. 3 caption for information.

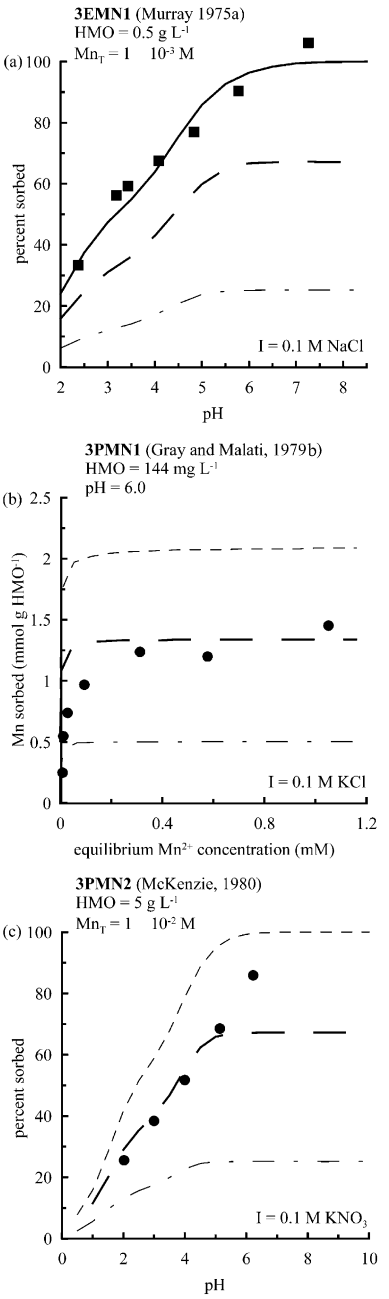

Fig. 9. Please refer to Fig. 3 caption for information.

notable successes of the sorption model. Three data sources were available for Cu; the best estimates of log K values determined using the relatively larger number of sources predicted all sorption data well. This result also suggests that the best α value of 0.64 and best log K values were appropriate for the HMO solids for which these parameters were unknown. Model predictions over range of α values shown in Fig. 7(j) (Stroes-Gascoyne et al., 1987) envelop most of the experimental data for HMO prepared by the redox method. All Pb data were predicted reasonably well. Evidence suggests that Pb forms multi-nuclear surface complexes (Manceau et al., 1992b); however, the model provides a satisfactory fit to the data using the chosen surface site types. The applicability of the Pb sorption model to a natural system is illustrated in Fig. 11(d) (Nelson et al., 1999). Evidence suggests that Pb sorption on biotic HMO is generally greater than that on abiotic HMO (Nelson et al., 1999). Data compiled for the sorption model were determined in abiotic systems, however. Lead sorption on biotic HMO was underpredicted by the model at high sorbate to sorbent ratios, but predicted values generally fell between biotic and abiotic experimental data. Lead, Co and Mn may be incorporated into HMO by processes other than sorption. However, general agreement between experimental data and model predictions suggests that the model reasonably estimates metal partitioning for these metals.

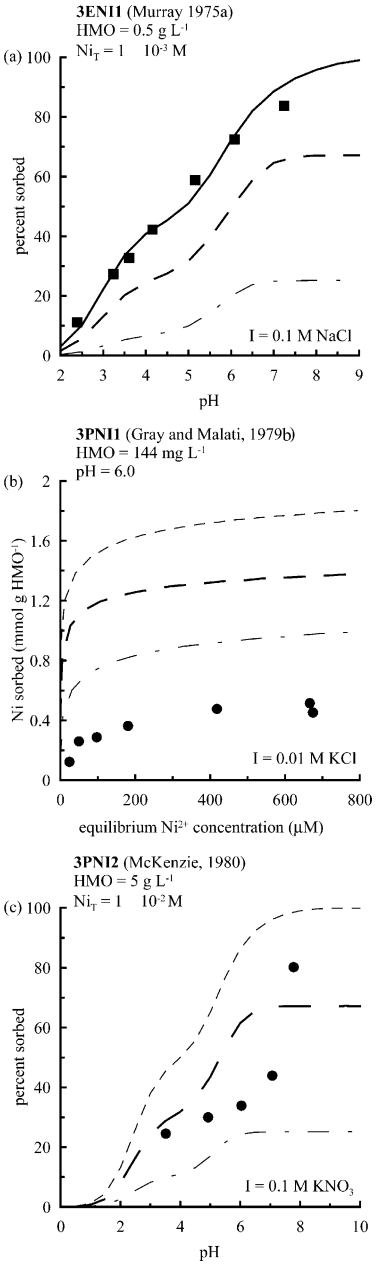

Fig. 10. Please refer to Fig. 3 caption for information.

Inconsistent or poor model predictions generally resulted from limited data availability. Both titration data and cation sorption data for the alkaline earth cations were provided in only one source (Murray, 1974, 1975a). Additionally, sorption edges for the individual metals contained very few data points. Inclusion of the surface species $\equiv XOHMe^{2+}$ used by Dzombak and Morel (1990) to model alkaline earth cation sorption on HFO did not result in a significantly better fit to the experimental data for Ba, Ca, Mg or Sr. For Ba and Ca, only the surface species $\equiv XOMe^{+}$ was significant in fitting the sorption data; inclusion of the species $\equiv XOMeOH$ did not significantly improve the data fits. Agreement between experimental data and model predictions for predicted Ba and Ca sorption data sets was inconsistent; however, the inclusion of additional data in the model may result in a more accurate description of Ba and Ca sorption on HMO. In contrast, both $\equiv XOMe^{+}$ and $\equiv XOMeOH$ species were significant in fitting Mg and Sr data. Data were fit well and additional data without supporting titration data were predicted well using the best α and best log K values. Cadmium and Nickel data were underpredicted by the model. Ni data were also underpredicted, to a greater degree, by Pretorius and Linder (2001). Zinc data were fit well, but the model's ability to predict additional sorption data was inconsistent. Inconsistencies between measured and predicted data were most apparent for sorption isotherm data. Isotherm data span a range of sorbate to sorbent ratios, and one set of log K values may be insufficient (Benjamin and Leckie, 1981). Only for metals for which more than one sorption data set was available was variability in the sorbate to sorbent ratios reflected in the best estimate log K values. Additionally, recent work suggests that the structure of birnessite changes with changing pH (Lanson et al., 2000), which has clear implications for fitting pH-dependent data.

With a paucity of available data sets, the precision and accuracy of the best estimate log K values determined with the model may be inadequate. More precise parameter values may be obtained with additional data sets. However, it remains difficult to paramaterize all variability among HMO solids.

Best α and best estimate cation surface complexation constant values were used to predict sorption edges at $I = 0.1$ M and fixed HMO and total metal concentrations of 10 mg l^{-1} and 1×10^{-6} M, respectively. The resulting curves are shown in Fig. 14. From these simulations the following sorption affinity sequence was

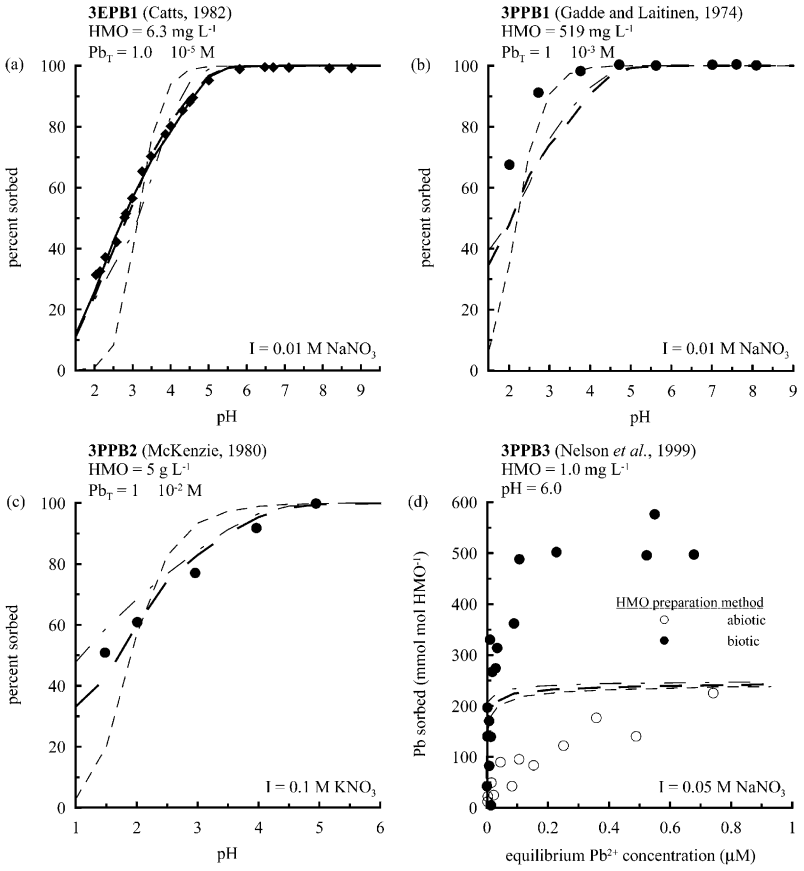

Fig. 11. Please refer to Fig. 3 caption for information.

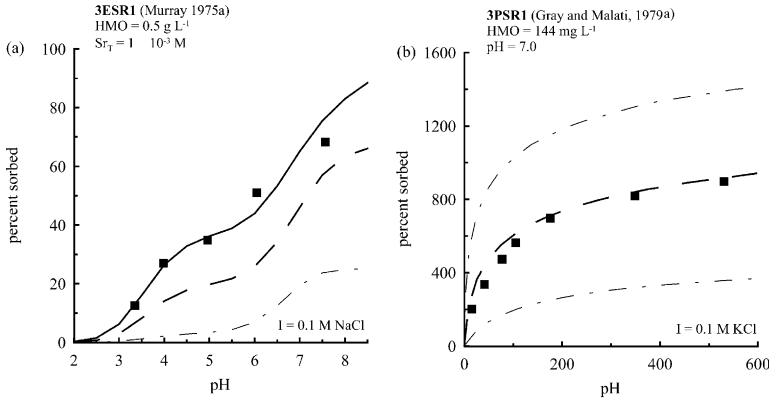

Fig. 12. Please refer to Fig. 3 caption for information.

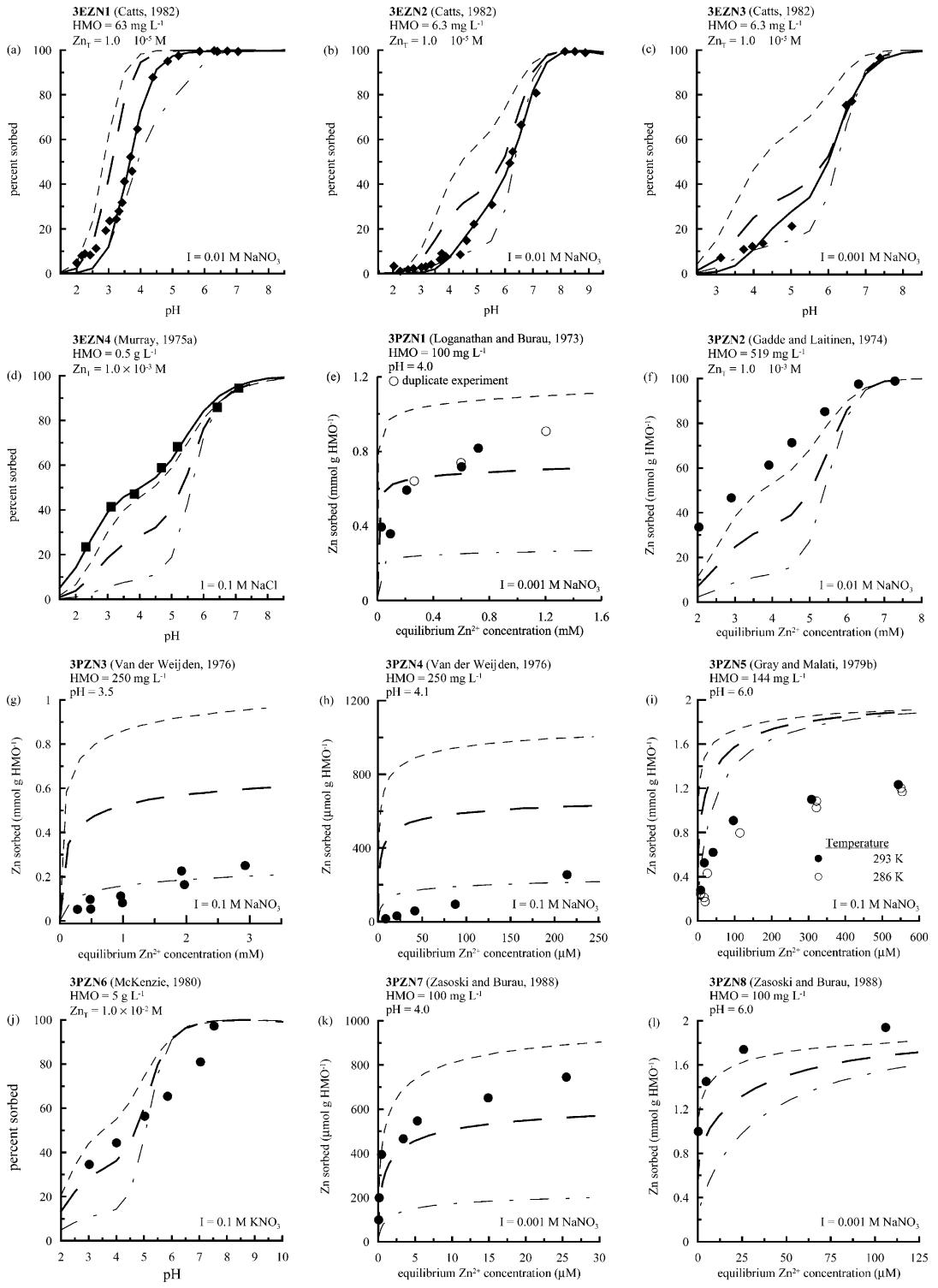

Fig. 13. Please refer to Fig. 3 caption for information.

determined for divalent metal cations on HMO: $Mg^{2+} < Ca^{2+} < Sr^{2+} < Cd^{2+} < Ni^{2+} < Zn^{2+} < Ba^{2+} < Cu^{2+} < Co^{2+} < Mn^{2+} < Pb^{2+}$. This sequence is similar to that reported for Fe oxides, with the exceptions of Mn^{2+}, Co^{2+} and Ba^{2+}, which adsorb more strongly on HMO.

Linear free energy relationships (LFER), or the correlation between first hydrolysis constants for aqueous species and the corresponding surface complexation constants, have been established for ion sorption on HFP (Dzombak and Morel, 1990) and goethite (Mathur, 1995). LFERs can be used to extend results from a limited data set to other metals. A comparison between the best HMO surface complexation constants determined for log K_{XOMe+} and log K_{XOMeOH} and metal hydrolysis constants is shown in Fig. 15. The general data trend and several data points suggest a LFER. However, this assumption may be limited for HMO by possible ion exchange reactions, limited available data for data fitting, or surface oxidation processes not described by the surface reactions chosen. Protons released to metal adsorbed ratios of close to 1 for Cu^{2+}, Mn^{2+}, Ni^{2+}, Pb^{2+}, and Zn^{2+} have been reported (Murray, 1975a; McKenzie, 1979). In contrast, a ratio of protons released to metal adsorbed of 0.3 for the alkaline earth cations was reported in Murray, (1975a), suggesting that a significant amount of the alkaline earth cations sorb at the HMO surface without proton exchange at a specific reaction site. A plot of the optimal log K_{XOMe+} values determined for Murray (1975a) as a function of crystal radius is shown in Fig. 16. Surface

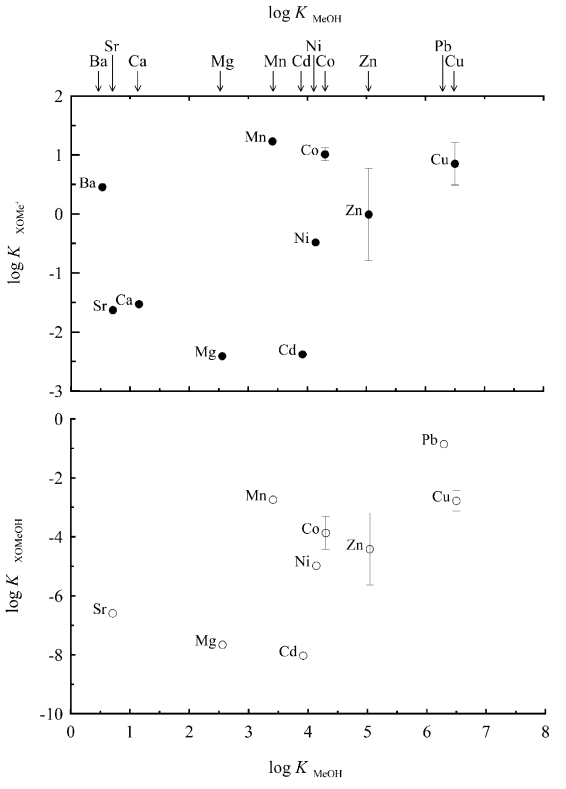

Fig. 15. Best ≡XOMe$^+$ and ≡XOMeOH surface complexation constants, $I=0$, as a function of the first hydrolysis constant (log K_{MeOH}). Error bars are shown at the 95% confidence level.

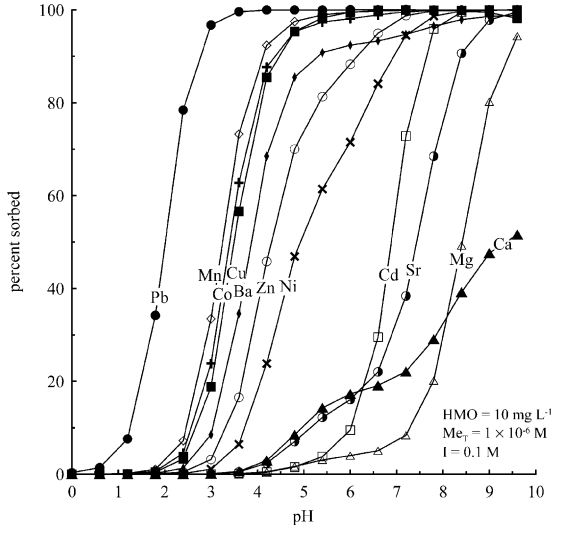

Fig. 14. Predicted sorption edges at $I=0$ for Ba, Ca, Cd, Co, Cu, Mg, Mn, Ni, Pb, Sr, and Zn using the best estimate surface complexation constants and fixed HMO and total metal concentrations of 10 mg l^{-1} and 1×10^{-6} M, respectively.

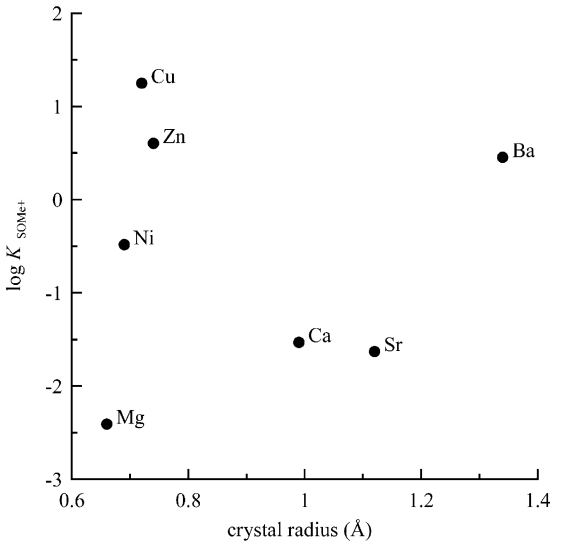

Fig. 16. Optimal log K_{XOMe+} values (Murray, 1974) as a function of crystal radius (Å) for Ba, Ca, Cu, Mg Ni, Sr, and Zn.

complexation constants for the transition metals Cu, Ni and Zn appear to have little dependence on ion size. However, there appears to be a linear relationship between surface complexation constants determined using the sorption model and crystal radius for the alkaline earth cations. A larger partition coefficient is expected for a larger cation with a smaller hydrated radius, which is consistent with the observed data trend.

If a LFER is assumed for the transition metals, Fig. 15 suggests that Cd data are underpredicted and Mn, Co and Pb data are overpredicted by the sorption model. Limited data sets were available for determining best surface complexation constants for Cd, Mn and Pb, however, which makes it difficult to judge the accuracy and precision of the resulting values. Additionally, surface processes not described by the sorption model may occur for Mn, Co and Pb. A ratio of protons released to Mn adsorbed consistently slightly higher than 1 has been reported (McKenzie, 1979), possibly due to Mn entering vacant Mn(II) sites in the crystal lattice. However, this effect was not sufficient to explain the relatively high amount of Mn sorption observed. The relatively high release of Mn to solution with sorption of Co (Loganathan and Burau, 1973), could result from substitution of Co(II) for structural Mn (III) and the subsequent oxidation of Co(II) to Co(III) (McKenzie, 1970). Theoretical calculations supported the oxidation of Co at the HMO surface and the presence of Co (III) has been confirmed by X-ray photoelectron spectroscopy (XPS) data (Murray and Dillard, 1979). Similar theoretical calculations support the oxidation of Pb (II) to Pb(IV) at the HMO surface (Murray and Dillard, 1979); however, this result is inconsistent with reported protons released to metal adsorbed ratios close to 1. The authors present the best estimates of cation surface complexation constants for all metals, including the alkaline earth cations, in Table 5. However, because it is not presently possible to distinguish between sorption and sorption plus oxidative mechanisms, the authors caution against assuming a LFER, or consistent behavior for sorption of all metals on HMO.

4. Summary and Conclusions

The diffuse double layer SCM, a two-site model, and titration data sets from 7 sources were used to determine HMO surface acidity constants and the range of α values that describe the fractions of the two site types for different HMO preparations. Good fits to cation sorption data using the HMO surface acidity constants were obtained where adequate data were available. The resulting cation surface complexation constants were used along with the range of α values to predict, with encouraging results, a number of cation sorption data sets where the surface characteristics of the HMO were less well defined. It is clear, however, that additional data describing surface characteristics of and sorption onto both synthetic and natural Mn oxides are necessary for a complete evaluation of the surface complexation approach. Considering the variability among currently available surface data for HMO solids, the modeler is faced with a dilemma when choosing a general modeling approach. One approach is to individually parameterize each data set, which may result in good model fits but also in uncertain values of log K, for which applicability to additional HMO phases is not well defined. The other approach, as was taken here, is to model consistently with fixed parameters such as pH_{IEP}, specific surface area, and total surface site density. Variability resulting from data collection, data interpretation, and inherent variability in the solid phase is thus contained in the precision of the log K values. Using a range of available data, the authors have provided a set of internally consistent surface complexation constants for HMO and the diffuse double layer SCM for modeling systems where HMO is an important scavenging phase.

Acknowledgements

The authors would like to thank David Dzombak for his helpful comments on an earlier draft.

Appendix 1. Optimal HMO Surface Acidity Constants, $I = 0$ (see ID and corresponding data sources in Table 1)

ID	pH_{IEP} correction	α	log $K_{a2\ (XOH)}$	σ_{log} K	log $K_{a2\ (YOH)}$	σ_{log} K
3T1	adjusted to $pH_{IEP} = 2.2$	1.0	−0.899	0.009	–[a]	
3T2			−0.770	0.008		
3T3			−1.397	0.008		
3T4			−2.098	0.009		
3T5			−2.753	0.015		
3T6	adjusted to $pH_{IEP} = 2.2$	0.24	−1.705	0.015	−5.994	0.010
3T7			−2.401	0.015	−6.308	0.010
3T8			−2.875	0.016	−6.256	0.011
3T9			−3.114	0.014	−6.173	0.010
3T10	adjusted to $pH_{IEP} = 2.2$	0.66	−1.392	0.020	−4.107	0.041
3T11			−1.675	0.015	−4.004	0.045
3T12	adjusted to $pH_{IEP} = 2.2$	0.57	−3.000	0.005	−5.428	0.033
3T13			−2.944	0.006	−5.821	0.019
3T14			−3.290	0.005	−6.095	0.017
3T15	adjusted to $pH_{IEP} = 2.2$	0.50	−2.568	0.011	−5.719	0.026
3T16			−2.621	0.011	−6.352	0.019
3T17			−2.436	0.014	−5.940	0.026
3T18	adjusted to $pH_{IEP} = 2.2$	0.52	−2.193	0.013	−5.916	0.032
3T19			−2.436	0.013	−5.838	0.032
3T20			−2.376	0.012	−5.879	0.033
3T21	No adjustment	1.0	−2.806	0.006	–	

[a] Dash lines indicate no estimate of log K from data fit.

Appendix 2. Error Estimates for HMO Cation Surface Complexation Constants, $I = 0$

Surface species		Ba^{2+}	Ca^{2+}	Cd^{2+}	Co^{2+}		Cu^{2+}		Mg^{2+}	Mn^{2+}	Ni^{2+}	Pb^{2+}	Sr^{2+}	Zn^{2+}	
		log K	log K	log K	log K		log K		log K	log K	log K	log K	log K	log K	
≡XOMe$^+$	Confidence Level (%)	0.454	−1.53	−2.38	1.01		0.850		−2.41	1.23	−0.483	–[a]	−1.63	−0.0101	
					(+)	(−)	(+)	(−)						(+)	(−)
	99				1.17	0.844	1.41	0.287						1.42	−1.44
	95				1.12	0.893	1.21	0.491						0.769	−0.790
	90				1.10	0.914	1.13	0.568						0.566	−0.586
	80				1.08	0.936	1.06	0.644						0.392	−0.412
≡XOMeOH		–	–	−8.03	−3.87		−2.76		−7.66	−2.74	−4.98	−0.857	−6.59	−4.42	
					(+)	(−)	(+)	(−)						(+)	(−)
	99				−3.00	−4.74	−2.19	−3.33						−1.61	−7.22
	95				−3.31	−4.42	−2.41	−3.10						−3.20	−5.63
	90				−3.43	−4.30	−2.49	−3.02						−3.59	−5.24
	80				−3.55	−4.19	−2.57	−2.95						−3.88	−4.95
≡YOMe$^+$		–	–	−3.50	–		−0.962		–	–	–	3.35	–	–	
							(+)	(−)							
	99						19.7	−21.6							
	95						3.15	−5.08							
	90						1.08	−3.01							
	80						0.0351	−1.96							
≡YOMeOH		–	–	−8.48	–		−5.62		–	–	–	−1.58	–	log K = −70.55	
							(+)	(−)						(+)	(−)
	99						−3.25	−7.99						15.7	−30.8
	95						−4.59	−6.65						−2.90	−12.2
	90						−4.92	−6.32						−5.24	−9.85
	80						−5.17	−6.07						−6.42	−8.67

[a] Dash lines indicate no estimate of log K from data fit.

References

Allison, J.D., Brown, D.S., Novo-Gradac, K.J., 1991. MINTEQA2/PRODEFA2, A geochemical assessment model for environmental systems: Version 3.0 User's Manual. U.S. Environmental Protection Agency, Athens, GA.

Appelo, C.J., Postma, D., 1999. A consistent model for surface complexation on birnessite (-MnO_2) and its application to a column experiment. Geochim. Cosmochim. Acta 63, 3039–3048.

Balistrieri, L.S., Murray, J.W., 1982. The surface chemistry of $dMnO_2$ in major ion seawater. Geochim. Cosmochim. Acta 46, 1041–1052.

Benjamin, M.M., Leckie, J.O., 1981. Multiple-site adsorption of Cd, Cu, Zn, and Pb on amorphous iron oxyhydroxide. J. Coll. Interface Sci. 79, 209–221.

Burns, R.G., Burns, V.M., 1979. Manganese oxides. In: Burns, R.G. (Ed.), Marine Minerals. Mineralogical Society of America, Washington, DC, pp. 1–46.

Catts, J.G., 1982. Adsorption of Cu, Pb and Zn onto Birnessite. Ph.D. thesis, Colorado School of Mines.

Catts, J.G., Langmuir, D., 1986. Adsorption of Cu, Pb and Zn by dMnO2: applicability of the site binding-surface complexation model. Appl. Geochem. 1, 255–264.

Christl, I., Kretzschmar, R., 1999. Competitive sorption of copper and lead at the oxide–water interface: implications for surface site density. Geochim. Cosmochim. Acta 63, 2929–2938.

Davis, J.A., 1977. Adsorption of trace metals and complexing ligands at the oxide/water interface. Ph.D. thesis, Stanford Univ.

Davis, J.A., Kent, D.B., 1990. Surface complexation modeling in aqueous geochemistry. In: Hochella, M.F., White, A.F. (Eds.), Reviews in Mineralogy. Mineralogical Society of America, Washington, D.C, pp. 177–260.

Davis, J.A., Coston, J.A., Kent, D.B., Fuller, C.C., 1998. Application of the surface complexation concept to complex mineral assemblages. Environmental Science & Technology 32, 2820–2828.

Drits, V.A., Silvester, E., Gorshkov, A.I., Manceau, A., 1997. Structure of synthetic monoclinic Na-rich birnessite and hexagonal birnessite: I. Results from X-ray diffraction and selected-area electron diffraction. Am. Mineral. 82, 946–961.

Dzombak, D.A., Morel, F., 1990. Surface Complexation Modeling : Hydrous Ferric Oxide. Wiley, New York.

Fu, G., Allen, H.E., Cowan, C.E., 1991. Adsorption of cadmium and copper by manganese oxide. Soil Sci. 152, 72–81.

Fuller, C.C., Davis, J.A., 1989. Influence of coupling of sorption and photosynthetic processes on trace-element cycles in natural-waters. Nature 340, 52–54.

Gadde, R.R., Laitinen, H.A., 1974. Studies of heavy metal adsorption by hydrous iron and manganese oxides. Anal. Chem. 46, 2022–2026.

Giovanoli, R., Stähli, E., Feitknecht, W., 1970a. Über oxidhydroxide des vierwertigen mangans mit schichtengitter. 1. Natriummangan(II,III)manganat(IV). Helv. Chim. Acta 53, 209–220.

Goldberg, S., 1998. Ion adsorption at the soil particle-solution interface: Modeling and mechanisms. In: Huang, P.M., Senesi, N., Buffle, J. (Eds.), Structure and Surface Reactions of Soil Particles. John Wiley & Sons Ltd., pp. 378–412.

Gray, M.J., Malati, M.A., 1979a. Adsorption from aqueous solution by d-manganese dioxide I. Adsorption of the alkaline-earth cations. J. Chem. Tech. Biotechnol. 29, 127–134.

Gray, M.J., Malati, M.A., 1979b. Adsorption from aqueous solution by d-manganese dioxide II. Adsorption of some heavy metal cations. J. Chem. Tech. Biotechnol. 29, 135–144.

Gray, M.J., Malati, M.A., Rophael, M.W., 1978. The point of zero charge of manganese dioxides. J. Electroanal. Chem. 89, 135–140.

Hamilton, W.C., 1965. Significance tests on the crystallographic R factor. Acta Cryst. 18, 502–510.

Herbelin, A.L., Westall, J.C., 1996. FITEQL: A computer program for determination of chemical equilibrium constants from experimental data. Department of Chemistry, Oregon State University, Corvallis, OR.

Honeyman, B.D., Santschi, P.H., 1988. Metals in aquatic systems. Environ. Sci. Technol. 22, 862–871.

Hugheey, J.E., Keiter, E.A., Keiter, R.L., 1993. Inorganic Chemistry: Principles of Structure and Reactivity. Harper Collins College Publishers, New York, NY.

Jenne, E.A., 1968. Controls on Mn, Fe, Co, Ni, Cu and Zn concentrations in soils and water: the significant role of hydrous Mn and Fe oxides. In: Baker, R.A. (Ed.), Trace Inorganics in Water. American Chemical Society, Washington, D.C, pp. 337–387.

Lanson, B., Drits, V.A., Silvester, E., Manceau, A., 2000. Structure of H-exchanged hexagonal birnessite and its mechanism of formation from Na-rich monoclinic buserite at low pH. Am. Mineral. 85, 826–838.

Lofts, S., Tipping, E., 1998. An assemblage model for cation binding by natural particulate matter. Geochim. Cosmochim. Acta 62, 2609–2625.

Loganathan, P., Burau, R.G., 1973. Sorption of heavy metal ions by a hydrous manganese oxide. Geochim. Cosmochim. Acta 37, 1277–1293.

Manceau, A., Gorshkov, A.I., Drits, V.A., 1992a. Structural chemistry of Mn, Fe, Co and Ni in manganese hydrous oxides: Part II. Information from EXAFS spectroscopy and electron and X-ray diffraction. Am. Mineral. 77, 1144–1157.

Manceau, A., Charlet, L., Boisset, M.C., Didier, B., Spaldini, L., 1992b. Sorption and speciation of heavy metals on hydrous Fe and Mn oxides. From microscopic to macroscopic. Appl. Clay Sci. 7, 201–223.

Mathur, S.M., 1995. Development of a Database for Ion Sorption on Goethite Using Surface Complexation Modeling. M.S. thesis, Carnegie Mellon Univ.

McKenzie, R.M., 1970. The reaction of cobalt with manganese dioxide minerals. Aust. J. Soil Res. 8, 97–106.

McKenzie, R.M., 1979. Proton release during adsorption of heavy metal ions by a hydrous manganese dioxide. Geochim. Cosmochim. Acta 23, 1855–1857.

McKenzie, R.M., 1980. The adsorption of lead and other heavy metals on oxides of manganese and iron. Aust. J. Soil Res. 18, 61–75.

McKenzie, R.M., 1981. The surface charge on manganese dioxides. Aust. J. Soil Res. 19, 41–50.

Morel, F.M.M., 1983. Principles of Aquatic Chemistry. John Wiley & Sons, New York.

Morgan, J.J., Stumm, W., 1964. Colloid-chemical properties of manganese dioxide. J. Coll. Sci. 19, 347–359.

Murray, J.W., 1974. The surface chemistry of hydrous manganese oxide. J. Coll. Interface Sci. 46, 357–371.

Murray, J.W., 1975a. The interaction of metal ions at the manganese dioxide-solution interface. Geochim. Cosmochim. Acta 39, 505–519.

Murray, J.W., 1975b. The interaction of cobalt with hydrous manganese dioxide. Geochim. Cosmochim. Acta 39, 635–647.

Murray, J.W., Dillard, J.G., 1979. The oxidation of cobalt(II) adsorbed on manganese dioxide. Geochim. Cosmochim. Acta 43, 781–787.

Nelson, Y.M., Lion, L.W., Ghiorse, W.C., Shuler, M.L., 1999. Production of biogenic Mn oxides by Leptothrix discophora SS-1 in a chemically defined growth medium and evaluation of their Pb adsorption characteristics. Appl. Environ. Microbiol. 65, 175–180.

Paulson, A.J., 1996. Fate of metals in surface waters of the Coeur d'Alene Basin, Idaho. United States Department of the Interior Bureau of Mines Report of Investigations, Rept. 9620.

Post, J.E., 1999. Manganese oxide minerals: crystal structures and economic and environmental significance. Proc. Natl. Acad. Sci. USA 96, 3447–3454.

Pretorius, P.J., Linder, P.W., 2001. The adsorption characteristics of d-manganese dioxide: a collection of diffuse double layer constants for the adsorption of H+, Cu2+, Ni2+, Zn2+, Cd2+ and Pb2+. Appl. Geochem. 16, 1067–1082.

Ran, Y., Fu, J., 1999. Adsorption of Au(III) and Au(I) complexes on d-MnO2. Sci. China (Series D) 42, 172–181.

Schindler, P.W., Stumm, W. The surface chemistry of oxides, hydroxides, and oxide minerals. Aquatic Surface Chemistry. Chemical Processes at the Particle-Water Interface. Shimm, N. (Ed.). John Wiley & Sons, 83–110.

Shiller, A.M., Boyle, E., 1985. Dissolved zinc in rivers. Nature 317, 49–52.

Silvester, E., Manceau, A., Drits, V.A., 1997. Structure of synthetic monoclinic Na-rich birnessite and hexagonal birnessite: II. Results from chemical studies and EXAFS spectroscopy. Am. Mineral. 82, 962–978.

Smith, R.W., Jenne, E.A., 1991. Recalculation, evaluation, and prediction of surface complexation constants for metal adsorption on iron and manganese oxides. Environ. Sci. Technol. 25, 525–531.

Sposito, G., 1983. On the surface complexation model of the oxide–aqueous solution interface. J. Coll. Interface Sci. 91, 329–340.

Stroes-Gascoyne, S., Kramer, J.R., Snodgrass, W.J., 1987. Preparation, characterization and aging of d-MnO2, for use in trace metal speciation studies. Appl. Geochem. 2, 217–226.

Stumm, W., Huang, C.P., Jenkins, S.R., 1970. Specific chemical interaction affecting the stability of dispersed systems. Croat. Chem. Acta 42, 223–244.

Tessier, A., Fortin, D., Belzile, N., DeVitre, R.-R., Leppard, G.G., 1996. Metal sorption to diagenetic iron and manganese oxyhydroxides and associated organic matter: narrowing the gap between field and laboratory measurements. Geochim. Cosmochim. Acta 60, 387–404.

Turner, D.R., Sassman, S.A., 1996. Approaches to sorption modeling for high-level waste performance assessment. J. Contam. Hydrol. 21, 311–332.

Van der Weijden, C.H., 1976. Experiments on the uptake of zinc and cadmium by manganese oxides. Mar. Chem. 4, 377–387.

Venema, P., Hiemstra, T., van Riemsdijk, W.H., 1996. Comparison of different site binding models for cation sorption: Description of pH dependency, salt dependency, and cation-proton exchange. J. Coll. Interface Sci. 181, 45–59.

Wen, X.H., Du, Q., Tang, H.X., 1998. Surface complexation model for the heavy metal adsorption on natural sediment. Environ. Sci. Technol. 32, 870–875.

Westall, J., Hohl, H., 1980. Comparison of electrostatic models for the oxide-solution interface. Adv. Coll. Interface Sci. 12, 265–294.

Yates, D.E., 1975. The Structure of the Oxide/Aqueous Electrolyte Interface. Ph.D., Univ. Melbourne.

Zasoski, R.J., Burau, R.G., 1988. Sorption and sorptive interaction of cadmium and zinc on hydrous manganese oxide. Soil Sci. Soc. Am. J. 52, 81–87.